

Geochemistry, Geophysics, Geosystems

RESEARCH ARTICLE

10.1029/2019GC008654

Key Points:

- Baffin Island-West Greenland high-³He/⁴He lavas are more geochemically depleted than any other high-³He/⁴He lavas globally
- The isotopic composition of the high-³He/⁴He mantle source in the Iceland plume has evolved through time
- Baffin Island and West Greenland primary melts record hotter temperatures than high-MgO MORB, consistent with a deep, dense plume source

Supporting Information:

- Supporting Information S1
- Figure S1
- Figure S2
- Figure S3
- Figure S4
- Table S1
- Table S2

Correspondence to:

L. N. Willhite,
lnw@umd.edu

Citation:

Willhite, L. N., Jackson, M. G., Blichert-Toft, J., Bindeman, I., Kurz, M. D., Halldórrsson, S. A., et al. (2019). Hot and heterogenous high-³He/⁴He components: New constraints from proto-Iceland plume lavas from Baffin Island. *Geochemistry, Geophysics, Geosystems*, 20, 5939–5967. <https://doi.org/10.1029/2019GC008654>

Received 23 AUG 2019

Accepted 3 NOV 2019

Accepted article online 11 NOV 2019

Published online 10 DEC 2019

Hot and Heterogenous High-³He/⁴He Components: New Constraints From Proto-Iceland Plume Lavas From Baffin Island

Lori N. Willhite¹ , Matthew G. Jackson¹ , Janne Blichert-Toft² , Ilya Bindeman³ , Mark D. Kurz⁴, Sæmundur A. Halldórrsson⁵, Sunna Harðardóttir⁵, Esteban Gazel⁶ , Allison A. Price¹ , and Benjamin L. Byerly¹

¹Department of Earth Science, University of California Santa Barbara, Santa Barbara, CA, USA, ²Laboratoire de Géologie de Lyon, Ecole Normale Supérieure de Lyon, CNRS UMR 5276, Université de Lyon, Lyon, France, ³Department of Earth Sciences, University of Oregon, Eugene, OR, USA, ⁴Marine Chemistry and Geochemistry, Woods Hole Oceanographic Institution, Woods Hole, MA, USA, ⁵NordVulk, Institute of Earth Sciences, University of Iceland, Reykjavík, Iceland, ⁶Department of Earth and Atmospheric Sciences, Cornell University, Ithaca, NY, USA

Abstract The Icelandic hotspot has erupted basaltic magma with the highest mantle-derived ³He/⁴He over a period spanning much of the Cenozoic, from the early-Cenozoic Baffin Island-West Greenland flood basalt province ($49.8 R_A$), to mid-Miocene lavas in northwest Iceland (40.2 to $47.5 R_A$), to Pleistocene lavas in Iceland's neovolcanic zone ($34.3 R_A$). The Baffin Island lavas transited through and potentially assimilated variable amounts of Precambrian continental basement. We use geochemical indicators sensitive to continental crust assimilation (Nb/Th, Ce/Pb, MgO) to identify the least crustally contaminated lavas. Four lavas, identified as “least crustally contaminated,” have high MgO (>15 wt.%), and Nb/Th and Ce/Pb that fall within the mantle range (Nb/Th = 15.6 ± 2.6 , Ce/Pb = 24.3 ± 4.3). These lavas have ⁸⁷Sr/⁸⁶Sr = 0.703008 – 0.703021 , ¹⁴³Nd/¹⁴⁴Nd = 0.513094 – 0.513128 , ¹⁷⁶Hf/¹⁷⁷Hf = 0.283265 – 0.283284 , ²⁰⁶Pb/²⁰⁴Pb = 17.7560 – 17.9375 , ³He/⁴He up to $39.9 R_A$, and mantle-like $\delta^{18}\text{O}$ of 5.03–5.21‰. The radiogenic isotopic compositions of the least crustally contaminated lavas are more geochemically depleted than Iceland high-³He/⁴He lavas, a shift that cannot be explained by continental crust assimilation in the Baffin suite. Thus, we argue for the presence of two geochemically distinct high-³He/⁴He components within the Iceland plume. Additionally, the least crustally contaminated primary melts from Baffin Island-West Greenland have higher mantle potential temperatures (1510 to 1630 °C) than Siqueiros mid-ocean ridge basalts (1300 to 1410 °C), which attests to a hot, buoyant plume origin for early Iceland plume lavas. These observations support the contention that the geochemically heterogeneous high-³He/⁴He domain is dense, located in the deep mantle, and sampled by only the hottest plumes.

1. Introduction

Helium isotopes provide an important tracer of ancient domains that have survived inside the Earth since its accretion. Helium isotopic ratios (normalized to Earth's atmosphere, ³He/⁴He = 1.384×10^{-6}) are relatively constant in mid-ocean ridge basalts, or MORB, ($8.8 \pm 2.1 R_A$, or ratio to atmosphere; Graham, 2002), which passively sample the upper mantle. However, plume-fed hotspots—such as Iceland, Hawaii, Samoa, and Galápagos—sample mantle domains with much higher ³He/⁴He ratios, thought to be located in the deep mantle ($>30 R_A$; e.g., Ellam & Stuart, 2004; Farley et al., 1992; Hilton et al., 1999; Jackson, Hart, et al., 2007; Kurz et al., 1982; Macpherson et al., 2005; Saal et al., 2007; Starkey et al., 2009). The highest observed mantle-derived ³He/⁴He (up to $49.8 \pm 0.7 R_A$) was found in the continental flood basalts associated with the Iceland plume at Baffin Island and West Greenland, erupted at ~60 Ma (Storey et al., 1998; Rizo et al., 2016; Starkey et al., 2009; Stuart et al., 2003; Graham et al., 1998). Elevated ³He/⁴He ratios were also identified in lavas related to the Iceland plume in east Greenland (Marty et al., 1998). Mid-Miocene lavas in northwest Iceland host the highest observed mantle-derived ³He/⁴He of any ocean island basalt (OIB) location ($47.5 R_A$, Harðardóttir et al., 2018; $40.2 R_A$, Mundl et al., 2017; $37.7 R_A$, Hilton et al., 1999). Modern Iceland lavas in the neovolcanic zone also have high ³He/⁴He (up to $34.3 R_A$; Macpherson et al., 2005). Therefore, the Iceland plume has hosted elevated ³He/⁴He over much of its history and, hence, is an ideal natural laboratory for studying the high-³He/⁴He mantle domain.

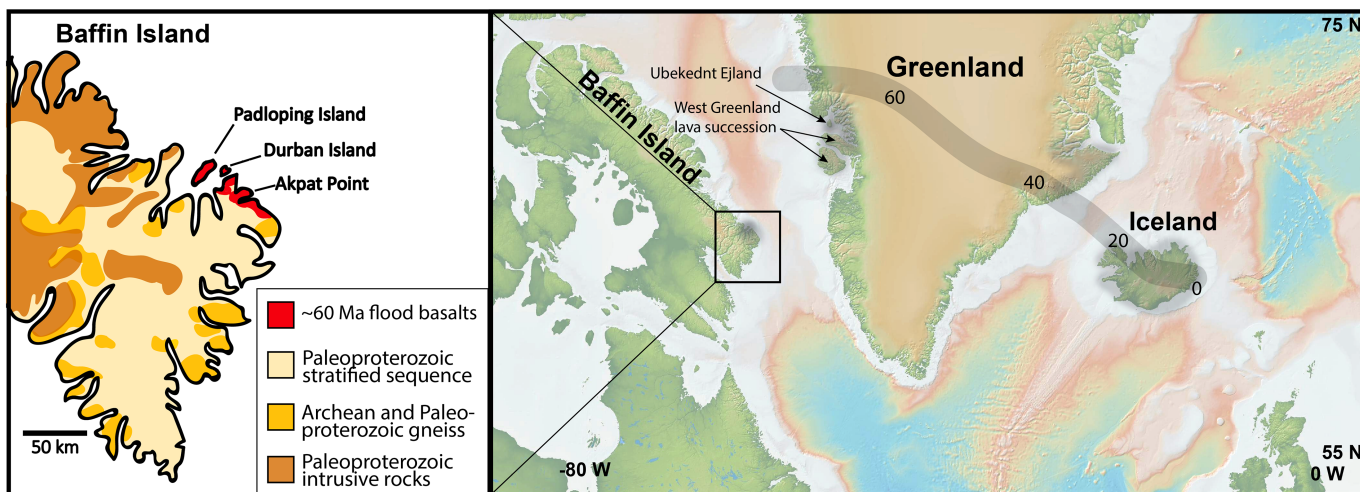


Figure 1. Map of Baffin Island, Greenland, and Iceland. General locations of Iceland plume-derived lavas are shaded in dark gray. The inset shows a simplified geologic map after Wheeler et al. (1996), including the locations of the lavas collected in this study: Padloping Island, Durban Island, and Akpat Point. The hotspot track is a synthetic track with the North American plate fixed through time (modified after Lawver & Müller, 1994) and is shown as the gray path. Also shown is the location of the ~60 Ma West Greenland succession samples compiled in Larsen and Pedersen (2009).

The high- $^3\text{He}/^4\text{He}$ mantle domain is ancient, requiring preservation in a region of the mantle that is relatively undegassed despite billions of years of mantle convective mixing, melting, and recycling (e.g., Class & Goldstein, 2005; Tackley, 2000; White, 2015; Zindler & Hart, 1986). Therefore, constraining the composition of the highest $^3\text{He}/^4\text{He}$ mantle reservoir observed in the rock record can provide important new insights into the accretionary history and early evolution of Earth's major chemical reservoirs. This study examines the geochemistry of flood basalts from Baffin Island, Canada (Figure 1), and West Greenland, providing new data—He-O-Sr-Nd-Hf-Pb isotopic compositions, as well as whole rock major and trace element concentrations—for 18 lavas from Baffin Island, in order to constrain the composition of the mantle domain with the highest observed $^3\text{He}/^4\text{He}$.

The Baffin Island and West Greenland lavas constitute a flood basalt province associated with the proto-Icelandic plume that erupted through Archean and Proterozoic continental crust, the assimilation of which could have overprinted their primary mantle signature (e.g., Day, 2016; Saunders et al., 1997). Therefore, we identify signatures of crustal assimilation in Baffin Island and West Greenland lavas using a suite of major and trace element filters—whole rock MgO, Ce/Pb, and Nb/Th—sensitive to continental crust assimilation, in order to isolate geochemical signatures of their mantle source. We show that, among high- $^3\text{He}/^4\text{He}$ lavas globally, the least contaminated lavas from Baffin Island have the most geochemically depleted $^{87}\text{Sr}/^{86}\text{Sr}$, $^{143}\text{Nd}/^{144}\text{Nd}$, and $^{176}\text{Hf}/^{177}\text{Hf}$, and the least radiogenic Pb isotopic compositions. Baffin Island-West Greenland lavas exhibit more geochemically depleted isotopic fingerprints than the high- $^3\text{He}/^4\text{He}$ lavas erupted in mainland Iceland, demonstrating temporal evolution of the high- $^3\text{He}/^4\text{He}$ component in the Iceland hotspot. The observation of two geochemically distinct, high- $^3\text{He}/^4\text{He}$ components in a single hotspot provides new constraints on the origin and evolution of mantle domains hosting high $^3\text{He}/^4\text{He}$.

2. Methods

2.1. Rock Collection, Preparation, and Analytical Methods

The 18 basalts examined in this study were collected at three locations on Baffin Island by Don Francis during the 2004 field season—Padloping Island, Akpat Point, and Durban Island (Figure 1 and Table S1 in the supporting information). Eleven of the 18 samples in this study have fresh volcanic glass on the margins of the basaltic pillows, a feature that has been identified previously in Baffin Island flood basalt lavas (e.g., Kent et al., 2004). The supporting information methods describe sample preparation and analytical techniques for whole rock major and trace element analyses (Table 1), whole rock isotopic analyses (He, Sr, Nd, Hf, Pb; Table 2), oxygen isotopic analyses of olivines (Table 3), and olivine compositions

Table 1
Major and Trace Elements of Baffin Island Lava and Reference Materials^a

	AK-1	AK-6	AK-8b	AK-9	AK-12	AK-13	AK-14	AK-18A	DB-9	DB-13	DB-14	DB-17
XRF												
SiO ₂ (wt.%)	45.05	43.80	45.83	45.40	45.30	44.88	44.87	44.81	44.16	44.69	45.10	46.52
TiO ₂	0.69	0.54	0.96	0.52	0.69	0.69	0.68	0.70	0.69	0.76	0.77	0.70
Al ₂ O ₃	11.54	8.63	11.04	9.83	11.51	11.61	11.47	11.76	9.86	10.95	10.92	11.60
FeO _T	10.43	10.57	10.88	10.51	10.37	10.60	10.46	10.47	10.53	10.82	10.76	10.13
MnO	0.17	0.17	0.18	0.17	0.17	0.18	0.17	0.18	0.17	0.18	0.18	0.17
MgO	19.31	24.28	19.85	23.63	19.40	19.53	19.65	19.43	23.01	20.81	20.76	18.90
CaO	10.25	7.27	9.41	8.21	10.51	10.07	10.28	10.04	8.26	9.09	9.06	9.76
Na ₂ O	1.22	0.88	1.30	0.98	1.26	1.27	1.15	1.26	0.88	1.09	1.04	1.23
K ₂ O	0.02	0.06	0.04	0.04	0.01	0.02	0.02	0.01	0.04	0.05	0.01	0.01
P ₂ O ₅	0.05	0.04	0.07	0.05	0.05	0.05	0.05	0.04	0.04	0.06	0.05	0.05
Total (majors only) ^b	98.74	96.24	99.55	99.32	99.29	98.88	98.79	98.71	97.67	98.46	98.64	99.08
LOI	0.22	3.27	0.00	0.13	0.32	0.00	0.55	0.59	1.37	0.47	0.65	0.05
Total (major, trace oxides, LOI) ^b	99.38	100.05	99.96	99.96	100.03	99.30	99.76	99.72	99.52	99.37	99.73	99.54
Olivine Fo# ^c												
XRF	87.0	83.7	89.6	89.0	87.2	87.1	87.6	87.3	88.0	87.5	87.0	88.8
Rb (ppm)	0.97	1.86	1.18	1.96	1.18	1.26	1.36	0.59	2.35	1.07	1.17	1.10
Sr	63.8	44.7	113.3	47.4	61.5	63.6	60.9	65.4	70.7	77.6	76.9	75.1
Zn	82.0	70.2	75.8	74.0	76.8	76.3	71.8	74.3	82.3	79.4	78.6	73.1
Ni	779	1094	849	1100	789	790	778	1038	878	871	763	
Cr	1605	2274	1398	2054	1630	1652	1648	1616	1805	1697	1711	1591
V	241	197	248	199	240	239	236	243	212	231	232	235
Cu	108.0	77.7	96.4	68.7	113.7	110.8	110.8	113.3	97.5	97.1	87.5	114.2
Ga	11.4	8.3	11.5	9.7	11.5	11.9	12.5	11.4	10.5	12.0	10.3	12.9
Ba	9.2	8.2	13.7	9.8	9.6	7.5	8.2	5.5	10.9	4.9	9.5	12.0
Y	16.8	11.9	15.9	12.3	16.2	15.7	15.4	16.7	13.4	16.5	15.2	15.6
Nb	0.50	0.10	1.00	0.00	0.60	0.20	0.40	1.19	0.60	0.89	0.10	0.96
Zr	36.4	28.9	53.1	26.0	36.8	36.9	35.4	36.3	39.2	42.4	41.1	36.6
ICP-MS												
Cs (ppm)	0.0027	0.014	0.0020	0.0004	0.0058	0.0011	0.0044	0.0043	0.0081	0.0029	0.0034	0.0055
Rb	0.26	1.08	0.28	0.15	0.30	0.20	0.23	0.42	0.95	0.12	0.17	0.26
Ba	6.04	6.21	11.18	4.77	5.76	4.87	5.84	7.36	7.32	6.55	7.89	9.60
Th	0.194	0.154	0.128	0.040	0.193	0.183	0.188	0.183	0.111	0.088	0.086	0.112
U	0.044	0.037	0.035	0.012	0.044	0.040	0.044	0.049	0.029	0.014	0.016	0.028
Nb	1.12	0.95	1.73	0.51	1.07	1.08	1.08	1.08	1.39	1.17	1.17	1.15
Ta	0.069	0.061	0.112	0.034	0.067	0.066	0.070	0.068	0.089	0.080	0.076	0.069
La	1.59	1.29	2.32	0.70	1.54	1.52	1.51	1.56	1.68	1.47	1.32	1.58
Ce	4.23	3.35	6.43	2.18	4.07	4.10	4.04	4.15	4.63	4.37	4.30	4.02
Pb	0.35	0.22	0.28	0.15	0.33	0.34	0.34	0.37	0.19	0.20	0.20	0.21
Pr	0.69	0.54	1.09	0.42	0.67	0.68	0.67	0.69	0.78	0.77	0.73	0.70
Nd	3.72	2.93	5.71	2.42	3.68	3.64	3.64	3.69	4.03	4.19	3.99	3.79
Sr	64.4	44.4	110.2	48.9	60.2	62.3	60.4	65.7	70.7	77.1	75.7	76.7
Zr	33.9	25.8	50.0	23.8	32.6	33.0	32.8	33.7	36.1	38.5	38.3	34.1
Hf	0.99	0.76	1.38	0.68	0.96	0.97	0.97	0.98	1.11	1.08	0.94	
Sm	1.54	1.18	2.10	1.11	1.52	1.51	1.52	1.48	1.54	1.69	1.61	1.48
Eu	0.65	0.48	0.83	0.46	0.62	0.63	0.63	0.64	0.60	0.66	0.65	0.62
Gd	2.33	1.72	2.69	1.71	2.23	2.27	2.27	2.28	2.09	2.31	2.27	2.22
Tb	0.46	0.33	0.49	0.34	0.43	0.44	0.43	0.44	0.39	0.44	0.42	0.41

Table 1 (continued)

	AK-1	AK-6	AK-8b	AK-9	AK-12	AK-13	AK-14	AK-18A	DB-9	DB-13	DB-14	DB-17
Dy	3.02	2.23	3.15	2.30	2.93	2.97	2.92	3.00	2.53	2.87	2.81	2.78
Ho	0.65	0.49	0.64	0.50	0.63	0.63	0.65	0.54	0.61	0.60	0.60	0.60
Y	16.2	12.0	16.0	12.8	15.7	15.8	15.6	16.2	13.5	15.1	14.6	15.0
Er	1.82	1.39	1.73	1.43	1.77	1.79	1.80	1.80	1.50	1.71	1.66	1.69
Tm	0.26	0.20	0.24	0.20	0.25	0.25	0.25	0.26	0.22	0.24	0.24	0.25
Yb	1.66	1.23	1.49	1.33	1.61	1.62	1.60	1.65	1.34	1.53	1.50	1.52
Lu	0.26	0.19	0.23	0.21	0.25	0.25	0.24	0.25	0.21	0.24	0.24	0.23
Sc	36.1	28.9	33.0	31.3	34.4	35.4	34.4	36.1	31.2	34.0	34.0	34.5
Ba/Th	31.2	40.4	87.1	119.8	29.8	26.5	31.0	40.1	65.8	74.5	91.4	85.9
Ce/Pb	12.1	15.5	22.9	14.7	12.3	12.2	11.8	11.2	24.0	22.2	21.7	19.4
Nb/U	25.6	25.8	50.0	42.1	24.3	26.8	24.7	21.8	47.2	86.4	74.4	40.6
Nb/Th	5.8	6.2	13.5	12.8	5.5	5.9	5.7	5.9	12.5	13.3	13.5	10.3
[La/Sm] _N	0.65	0.68	0.69	0.39	0.63	0.63	0.62	0.66	0.68	0.55	0.52	0.67
Rb/Cs	95.8	78.1	134.9	359.9	52.1	188.6	52.3	97.6	116.6	42.1	48.7	46.9
Ba/Rb	23.6	5.8	40.7	31.8	19.0	24.5	25.2	17.7	7.7	53.2	47.6	37.0
Th/U	4.4	4.2	3.7	3.3	4.4	4.5	4.3	3.7	3.8	6.5	5.5	3.9
	DB-19	PI-10	PI-15	PI-17	PI-18	PI-20	BCR-2	BCR-2	BCR-2	BHVO-2	BHVO-2	BHVO-2 publ
XRF												
SiO ₂ (wt.%)	46.11	46.26	44.59	46.28	45.73	45.59	53.96	54.46	54.93	50.04	50.23	
TiO ₂	1.29	1.00	0.75	0.86	0.84	0.83	2.28	2.30	2.30	2.78	2.77	
Al ₂ O ₃	11.38	12.85	10.60	12.18	11.83	11.61	13.56	13.62	13.71	13.68	13.61	
FeO _T	10.79	10.75	10.66	10.43	10.59	10.55	12.85	12.62	12.61	11.25	11.29	
MnO	0.18	0.18	0.17	0.17	0.17	0.17	0.20	0.20	0.20	0.17	0.17	
MgO	17.03	15.17	21.58	17.73	18.48	18.56	3.59	3.53	3.66	7.30	7.35	
CaO	9.23	10.86	8.94	10.08	9.77	9.62	7.15	7.16	7.24	11.51	11.54	
Na ₂ O	1.39	1.35	1.08	1.31	1.26	1.21	3.17	3.10	3.17	2.24	2.25	
K ₂ O	0.17	0.02	0.01	0.04	0.04	0.05	1.79	1.79	1.80	0.52	0.52	
P ₂ O ₅	0.12	0.07	0.06	0.07	0.07	0.07	0.35	0.35	0.37	0.26	0.27	
Total (majors only) ^b	97.71	98.50	98.44	99.16	98.79	98.26	98.92	99.13	100.00	99.74	100.00	
LOI	1.18	0.49	0.43	0.56	0.45	0.55	0.10	0.00	0.00	0.00	0.00	
Total (major, trace oxides, LOI) ^b	99.28	99.30	99.32	100.10	99.64	99.21	99.27	99.39				99.99
Olivine Fo# ^c	86.4	87.1	88.7	90.4	89.9	90.4						
XRF												
Rb (ppm)	3.38	1.97	1.07	0.97	1.56	1.84	47	47	46	11	9	
Sr	170.9	109.0	74.3	99.8	94.8	92.7	340	343	337	397	394	
Zn	81.3	77.9	85.9	74.1	77.9	77.1	133	130	130	105	104	
Ni	638	486	943	684	734	738	14	13	13	121	120	
Cr	1304	1016	1720	1415	1486	1470	9	12	16	283	287	
V	288	272	228	245	241	235	405	408	418	321	318	
Cu	79.7	119.1	86.2	93.0	83.9	87.6	20	19	20	130	129	
Ga	12.3	14.0	11.3	12.5	10.8	11.2	20	22	22	21	21	
Ba	74.8	23.0	6.4	18.2	22.6	22.1	676	678	684	139	131	
Y	24.7	18.6	14.8	17.5	15.8	16.7	36	36	36	26	26	
Nb	7.53	3.15	0.00	4.55	2.59	3.76	12	13	12	16	18	
Zr	80.8	54.2	39.8	50.0	49.1	49.4	182	181	187	168	171	
ICP-MS												

Table 1 (continued)

	DB-19	PI-10	PI-15	PI-17	PI-18	PI-20	BCR-2	BCR-2 publ	BHVO-2	BHVO-2 publ
Cs (ppm)	0.0070	0.0041	0.0032	0.0060	0.0055	0.0093	1.13	1.16	0.098	0.100
Rb	2.95	0.24	0.18	0.31	0.41	0.61	46.3	46.0	8.95	9.26
Ba	71.37	15.20	5.97	21.63	22.76	25.91	679	684	130	131
Th	0.713	0.294	0.098	0.416	0.410	0.392	6.18	5.83	1.26	1.22
U	0.146	0.043	0.018	0.054	0.049	0.063	1.54	1.68	0.41	0.41
Nb	7.85	3.62	1.36	4.26	4.16	4.12	12.6	12.4	19.4	18.1
Ta	0.460	0.211	0.087	0.250	0.242	0.239	0.81	0.79	1.27	1.15
La	6.56	3.51	1.63	3.67	3.18	3.25	26.1	25.1	15.7	15.2
Ce	14.12	8.48	4.69	8.35	8.01	7.93	51.1	53.1	36.3	37.5
Pb	0.80	0.38	0.19	0.36	0.34	0.34	10.0	10.6	1.58	1.65
Pr	1.99	1.31	0.79	1.22	1.10	1.13	6.57	6.83	5.17	5.34
Nd	9.18	6.35	4.32	5.92	5.36	5.51	27.0	28.3	23.3	24.3
Sr	170.7	110.1	74.2	100.7	92.3	91.3	347	337	396	394
Zr	80.1	53.7	38.2	48.9	46.8	46.9	188	187	173	171
Hf	2.06	1.47	1.05	1.31	1.28	1.29	4.81	4.97	4.40	4.47
Sm	3.04	2.26	1.64	2.05	1.87	1.89	7.01	6.55	6.45	6.02
Eu	1.08	0.89	0.64	0.78	0.73	0.74	2.15	1.99	2.24	2.04
Gd	3.84	2.96	2.25	2.69	2.54	2.52	7.11	6.81	6.64	6.21
Tb	0.69	0.53	0.42	0.50	0.47	0.48	1.17	1.08	1.04	0.94
Dy	4.45	3.49	2.74	3.27	3.07	3.10	7.09	6.42	5.87	5.28
Ho	0.95	0.74	0.58	0.69	0.65	0.66	1.42	1.31	1.08	0.99
Y	23.5	18.4	14.6	17.0	16.0	16.2	35.7	36.1	25.9	25.9
Er	2.62	2.04	1.64	1.93	1.81	1.84	3.87	3.67	2.67	2.51
Tm	0.37	0.30	0.23	0.27	0.26	0.26	0.55	0.53	0.34	0.33
Yb	2.35	1.80	1.45	1.71	1.64	1.65	3.38	3.39	2.01	1.99
Lu	0.36	0.28	0.24	0.27	0.25	0.26	0.52	0.505	0.29	0.28
Sc	34.3	38.9	33.4	37.0	35.5	35.7	34.3	33.5	31.7	31.8
Ba/Th	100.1	51.6	60.8	52.0	55.5	66.2	110	117	103	107
Ce/Pb	17.6	22.4	24.1	22.9	23.8	23.3	5.10	5.02	22.99	22.70
Nb/U	53.7	84.0	77.8	85.3	64.9	8.14	7.39	47.05	43.93	
Nb/Th	11.0	12.3	13.9	10.3	10.2	10.5	2.04	2.13	15.42	14.79
[La/Sm] _N	1.35	0.98	0.62	1.13	1.06	1.08	2.33	2.40	1.53	1.58
Rb/Cs	424.3	58.1	54.8	52.1	74.1	65.7	41.0	39.7	91.5	93.0
Ba/Rb	24.2	63.6	33.8	69.0	56.2	42.6	14.7	14.9	14.5	14.1
Th/U	4.9	6.8	5.6	7.6	8.4	6.2	4.0	3.5	3.1	3.0

^aMajors and some traces were analyzed by XRF at WSU. The other traces were analyzed by ICP-MS at WSU. Two USGS reference materials, BCR-2 and BHVO-2, were run together with the Baffin lavas as unknowns. These data are provided with preferred values from Jochum et al. (2016) (data are expressed with all Fe as FeO to facilitate comparison with new BCR-2 and BHVO-2 provided here).

^bTwo different totals are included for major element analyses. The first total includes major element analyses only. The second total includes major element analyses, LOI (loss on ignition), and the trace element totals expressed as oxides (and includes the following trace elements: Ni, Cr, Sc, V, Ba, Rb, Sr, Zr, Y, Nb, Ga, Cu, Zn, Pb, La, Ce, Th, Nd and U).

^cOlivine forsterite compositions are average values of multiple analyses of different olivine grains provided in Supporting Information Table S2.

(supporting information Table S2). Thin section images of all 18 samples are provided in the supporting information Figure S1.

Additionally, in supporting information methods section S2.1, a set of criteria are established for filtering Baffin Island and West Greenland lavas that have experienced crustal assimilation. In short, lavas are considered to have experienced crustal assimilation if they have $MgO < 10$ wt.% and/or Ce/Pb and/or Nb/Th ratios below values representative of the mantle (i.e., $Ce/Pb < 20$ and $Nb/Th < 13$).

3. Data and Results

3.1. Major Element and Primary Melt Compositions

Major element concentrations for the Baffin Island lavas in this study are shown in Figures 2 and 3 with previously analyzed Baffin Island and West Greenland flood basalt lavas. The lavas are visually fresh and have LOI (loss on ignition) < 1.4 wt.%, with the exception of one lava with LOI = 3.3 wt.% (Table 2). The new suite of lavas reported here are tholeiitic picrites with MgO contents ranging from 15–25 wt.% (Figure 2) (Le Bas et al., 1986; Francis, 1985). To illustrate differences in major element compositions between MORB and the Baffin Island-West Greenland flood basalts, we calculated primary melt compositions of the least contaminated and least evolved (only $MgO > 10$ wt.% are considered) Baffin Island and West Greenland lavas, as well as high- MgO (> 10 wt.%) Siqueiros MORB. Relatively few ($N = 9$) Baffin Island-West Greenland lavas remain after filtering for continental crust assimilation using the criteria established in section S2.1 in the supporting information. Primary melts are calculated for Siquieros, Baffin Island, and West Greenland lavas using the PRIMELT3 software assuming an Fe_2O_3/TiO_2 ratio of 0.5 (Herzberg & Asimow, 2015). Relative to MORB, the least contaminated Baffin Island-West Greenland primary melts have higher FeO , but lower Na_2O and Al_2O_3 , and generally lower CaO and SiO_2 . TiO_2 is not different between the two groups (Figure 3). The Baffin Island-West Greenland primary melts are highly magnesian, with calculated primary melt MgO ranging from 19–24 wt.%, which exceeds the range of calculated MgO (11–17 wt.%) in the MORB primary melts.

3.2. Olivine Major and Minor Element Compositions

Olivine forsterite content from the Baffin Island lavas examined here range from forsterite 79.3 to 92.8 for individual spot analyses of at least 10 grains from each of 18 different rock samples (Figure 4 and Table S2). High forsterite olivines in Baffin Island lavas were previously reported by Francis (1985), Yaxley et al. (2004), and Starkey et al. (2012), who found forsterite compositions up to 93.2, 92.9, and 93.0, respectively. Olivines in this suite of Baffin Island lavas have higher CaO for a given forsterite than olivines found in global mantle xenoliths (Hervig et al., 1986) and mantle xenoliths from Ubekendt Ejland, West Greenland, which sample the mantle beneath the Baffin Island-West Greenland flood basalts (Bernstein et al., 2006). The CaO content of olivine reflects equilibration temperature and pressure conditions (Köhler & Brey, 1990); the high olivine CaO for a given forsterite is typical of high-temperature, low-pressure magmatic olivine and suggests that the olivines in the Baffin Island lavas are likely to be magmatic in origin (e.g., Jackson & Shirey, 2011).

3.3. Trace Element Compositions

Primitive mantle-normalized (McDonough & Sun, 1995) trace element patterns, or spidergrams, are shown in Figure 5 for the Baffin Island lavas. While one sample (DB-19) has a slightly enriched rare earth element (REE) pattern ($[La/Sm]_N = 1.35$, where N denotes normalization to primitive mantle), four lavas (PI-10, PI-17, PI-18, and PI-20) have relatively flat light REE patterns ($[La/Sm]_N = 0.98\text{--}1.13$) and the remaining lavas have depleted light REE patterns ($[La/Sm]_N = 0.39\text{--}0.70$). Some of the relatively fluid mobile incompatible trace elements exhibit depletions in the lavas relative to elements of similar incompatibility during mantle melting, including Cs, Rb, K, and Pb, and in some cases U. Depletions in Pb are common in mantle-derived lavas (Hart & Gaetani, 2006) and reflect either the mantle source or residual sulfide. In contrast, depletion in U and alkalis may reflect loss of these elements during subaerial weathering. For example, 13 lavas exhibit Th/U greater than the chondritic primitive mantle composition (3.876 ± 0.016 ; Blichert-Toft et al., 2010), with one value as high as 8.4, which likely reflects loss of U relative to immobile Th during weathering. Evidence for alkali mobility is supported by departure of Baffin Island lavas from the canonical Ba/Rb

Table 2
New Sr, Nd, Hf, Pb, He, and O Isotopic Compositions of Baffin Island Lavas

Sample name	Location	Sample type ^a	$^{87}\text{Sr}/^{86}\text{Sr}$	2σ	$^{143}\text{Nd}/^{144}\text{Nd}$	2σ	$\varepsilon^{143}\text{Nd}^b$	$^{176}\text{Hf}/^{177}\text{Hf}$	2σ	$^{206}\text{Pb}/^{204}\text{Pb}$	2σ
AK-1	Akpat Pt.	Glass	0.703559	0.000006	0.512963	0.000006	6.5	0.283231	0.000004	17.6822	0.0013
AK-6	Akpat Pt.	Rock chips	0.703501	0.000006	0.512997	0.000003	7.2	0.283222	0.000005	17.6249	0.0009
AK-8b	Akpat Pt.	Rock chips	0.703099	0.000006	0.513128	0.000003	9.7	0.283266	0.000003	17.7560	0.0010
AK-9	Akpat Pt.	Rock chips	0.702995	0.000006	0.513174	0.000003	10.6	0.283287	0.000005	17.7715	0.0050
AK-9 fusion	Akpat Pt.	Glass	0.703579	0.000007	0.512954	0.000006	6.3	0.283234	0.000004	17.6890	0.0015
AK-12	Akpat Pt.	Glass	0.703579	0.000008	0.512957	0.000005	6.4	0.283212	0.000005	17.6601	0.0018
AK-13 ^d	Akpat Pt.	Glass									
AK-13 crush replicate ^d	Akpat Pt.	Glass									
AK-14	Akpat Pt.	Glass	0.703618	0.000021	0.512956	0.000006	6.4	0.283218	0.000005	17.6951	0.0028
AK-18a	Akpat Pt.	Glass	0.703635	0.000006	0.512952	0.000006	6.3	0.283229	0.000004	17.7029	0.0045
DB-9	Durban Is.	Rock chips	0.702997	0.000009	0.513135	0.000003	9.8	0.283272	0.000004	17.9507	0.0031
DB-13	Durban Is.	Glass	0.703021	0.000005	0.513102	0.000003	9.2	0.283265	0.000004	17.9317	0.0025
DB-14	Durban Is.	Glass	0.703021	0.000005	0.513097	0.000003	9.1	0.283284	0.000003	17.9297	0.0025
DB-17	Durban Is.	Rock chips	0.703228	0.000006	0.513104	0.000003	9.2	0.283230	0.000006	17.5114	0.0042
DB-17 fusion	Durban Is.	Rock chips	0.703946	0.000005	0.512937	0.000003	6.0	0.283144	0.000004	18.0095	0.0012
PI-10	Padloping Is.	Rock chips	0.703401	0.000005	0.513028	0.000003	7.8	0.283222	0.000004	17.9607	0.0032
PI-15	Padloping Is.	Glass	0.703008	0.000005	0.513094	0.000003	9.0	0.283279	0.000003	17.9375	0.0029
PI-17	Padloping Is.	Glass	0.703845	0.000006	0.512926	0.000003	5.8	0.283169	0.000004	17.7551	0.0013
PI-18	Padloping Is.	Glass	0.703848	0.000006	0.512920	0.000003	5.7	0.283169	0.000004	17.7542	0.0012
PI-20	Padloping Is.	Glass	0.703846	0.000006	0.512923	0.000003	5.7	0.283182	0.000003	17.7540	0.0015
BCR-2 ^e											
BCR-2 ^e											
BCR-2 ^{e,f}											
AGV-2 ^f											
AGV-2 ^f											
AGV-2 ^f											
BCR-2 ^g											
AGV-2 ^g											
Sample name		$^{207}\text{Pb}/^{204}\text{Pb}$	$^{208}\text{Pb}/^{204}\text{Pb}$	2σ	$^{207}\text{Pb}/^{206}\text{Pb}$	2σ	$^{208}\text{Pb}/^{206}\text{Pb}$	2σ	$^{18}\text{O oliv}$	$^{3}\text{He}/^{4}\text{He}^c$	1σ
AK-1	15.2945	0.0014	37.751	0.003	0.86496	0.00002	2.13501	0.00006	5.21	1.50	0.08
AK-6	15.2887	0.0010	37.664	0.003	0.86747	0.00002	2.13704	0.00008	5.33	2.9	0.8
AK-8b	15.3932	0.0009	37.532	0.002	0.86694	0.00001	2.11373	0.00004	5.03	39.9	0.5
AK-8b fusion											
AK-9	15.3812	0.0045	37.500	0.012	0.86557	0.00003	2.11018	0.00006		20.8	0.5
AK-9 fusion											
AK-12	15.2932	0.0015	37.738	0.004	0.86458	0.00003	2.13340	0.00006		56.6	1.1
AK-13 ^d	15.2930	0.0018	37.700	0.005	0.86600	0.00002	2.13480	0.00007		30.1	0.7
AK-13 crush replicate ^d											
AK-14	15.3013	0.0025	37.762	0.006	0.86470	0.00003	2.13396	0.00008	5.12	28.8	0.4
AK-18a	15.3128	0.0040	37.761	0.010	0.86499	0.00003	2.13315	0.00006		21.5	0.5
DB-9	15.4168	0.0030	37.717	0.008	0.85886	0.00004	2.10123	0.00010		13.3	0.7
DB-13	15.4291	0.0021	37.732	0.006	0.86044	0.00002	2.10434	0.00015		5.03	12.0
DB-14	15.4279	0.0030	37.735	0.007	0.86047	0.00004	2.10453	0.00008		5.09	10.1
Sample name		$^{207}\text{Pb}/^{204}\text{Pb}$	$^{208}\text{Pb}/^{204}\text{Pb}$	2σ	$^{207}\text{Pb}/^{206}\text{Pb}$	2σ	$^{208}\text{Pb}/^{206}\text{Pb}$	2σ	$^{18}\text{O oliv}$	$^{3}\text{He}/^{4}\text{He}^c$	1σ
AK-1	15.2945	0.0014	37.751	0.003	0.86496	0.00002	2.13501	0.00006	5.21	1.50	0.08
AK-6	15.2887	0.0010	37.664	0.003	0.86747	0.00002	2.13704	0.00008	5.33	2.9	0.8
AK-8b	15.3932	0.0009	37.532	0.002	0.86694	0.00001	2.11373	0.00004	5.03	39.9	0.5
AK-8b fusion											
AK-9	15.3812	0.0045	37.500	0.012	0.86557	0.00003	2.11018	0.00006		20.8	0.5
AK-9 fusion											
AK-12	15.2932	0.0015	37.738	0.004	0.86458	0.00003	2.13340	0.00006		56.6	1.1
AK-13 ^d	15.2930	0.0018	37.700	0.005	0.86600	0.00002	2.13480	0.00007		30.1	0.7
AK-13 crush replicate ^d											
AK-14	15.3013	0.0025	37.762	0.006	0.86470	0.00003	2.13396	0.00008	5.12	28.8	0.4
AK-18a	15.3128	0.0040	37.761	0.010	0.86499	0.00003	2.13315	0.00006		21.5	0.5
DB-9	15.4168	0.0030	37.717	0.008	0.85886	0.00004	2.10123	0.00010		5.10	13.3
DB-13	15.4291	0.0021	37.732	0.006	0.86044	0.00002	2.10434	0.00015		5.03	12.0
DB-14	15.4279	0.0030	37.735	0.007	0.86047	0.00004	2.10453	0.00008		5.09	10.1
Sample name		$^{207}\text{Pb}/^{204}\text{Pb}$	$^{208}\text{Pb}/^{204}\text{Pb}$	2σ	$^{207}\text{Pb}/^{206}\text{Pb}$	2σ	$^{208}\text{Pb}/^{206}\text{Pb}$	2σ	$^{18}\text{O oliv}$	$^{3}\text{He}/^{4}\text{He}^c$	1σ
AK-1	15.2945	0.0014	37.751	0.003	0.86496	0.00002	2.13501	0.00006	5.21	1.50	0.08
AK-6	15.2887	0.0010	37.664	0.003	0.86747	0.00002	2.13704	0.00008	5.33	2.9	0.8
AK-8b	15.3932	0.0009	37.532	0.002	0.86694	0.00001	2.11373	0.00004	5.03	39.9	0.5
AK-8b fusion											
AK-9	15.3812	0.0045	37.500	0.012	0.86557	0.00003	2.11018	0.00006		20.8	0.5
AK-9 fusion											
AK-12	15.2932	0.0015	37.738	0.004	0.86458	0.00003	2.13340	0.00006		56.6	1.1
AK-13 ^d	15.2930	0.0018	37.700	0.005	0.86600	0.00002	2.13480	0.00007		30.1	0.7
AK-13 crush replicate ^d											
AK-14	15.3013	0.0025	37.762	0.006	0.86470	0.00003	2.13396	0.00008	5.12	28.8	0.4
AK-18a	15.3128	0.0040	37.761	0.010	0.86499	0.00003	2.13315	0.00006		21.5	0.5
DB-9	15.4168	0.0030	37.717	0.008	0.85886	0.00004	2.10123	0.00010		5.10	13.3
DB-13	15.4291	0.0021	37.732	0.006	0.86044	0.00002	2.10434	0.00015		5.03	12.0
DB-14	15.4279	0.0030	37.735	0.007	0.86047	0.00004	2.10453	0.00008		5.09	10.1
Sample name		$^{207}\text{Pb}/^{204}\text{Pb}$	$^{208}\text{Pb}/^{204}\text{Pb}$	2σ	$^{207}\text{Pb}/^{206}\text{Pb}$	2σ	$^{208}\text{Pb}/^{206}\text{Pb}$	2σ	$^{18}\text{O oliv}$	$^{3}\text{He}/^{4}\text{He}^c$	1σ
AK-1	15.2945	0.0014	37.751	0.003	0.86496	0.00002	2.13501	0.00006	5.21	1.50	0.08
AK-6	15.2887	0.0010	37.664	0.003	0.86747	0.00002	2.13704	0.00008	5.33	2.9	0.8
AK-8b	15.3932	0.0009	37.532	0.002	0.86694	0.00001	2.11373	0.00004	5.03	39.9	0.5
AK-8b fusion											
AK-9	15.3812	0.0045	37.500	0.012	0.86557	0.00003	2.11018	0.00006		20.8	0.5
AK-9 fusion											
AK-12	15.2932	0.0015	37.738	0.004	0.86458	0.00003	2.13340	0.00006		56.6	1.1
AK-13 ^d	15.2930	0.0018	37.700	0.005	0.86600	0.00002	2.13480	0.00007		30.1	0.7
AK-13 crush replicate ^d											
AK-14	15.3013	0.0025	37.762	0.006	0.86470	0.00003	2.13396	0.00008	5.12	28.8	0.4
AK-18a	15.3128	0.0040	37.761	0.010	0.86499	0.00003	2.13315	0.00006		21.5	0.5
DB-9	15.4168	0.0030	37.717	0.008	0.85886	0.00004	2.10123	0.00010		5.10	13.3
DB-13	15.4291	0.0021	37.732	0.006	0.86044	0.00002	2.10434	0.00015		5.03	12.0
DB-14	15.4279	0.0030	37.735	0.007	0.86047	0.00004	2.10453	0.00008		5.09	10.1
Sample name		$^{207}\text{Pb}/^{204}\text{Pb}$	$^{208}\text{Pb}/^{204}\text{Pb}$	2σ	$^{207}\text{Pb}/^{206}\text{Pb}$	2σ	$^{208}\text{Pb}/^{206}\text{Pb}$	2σ	$^{18}\text{O oliv}$	$^{3}\text{He}/^{4}\text{He}^c</math$	

Table 2 (continued)

Sample name	$^{207}\text{Pb}/^{204}\text{Pb}$	$^{208}\text{Pb}/^{204}\text{Pb}$	$^{207}\text{Pb}/^{206}\text{Pb}$	$^{208}\text{Pb}/^{206}\text{Pb}$	$\delta^{18}\text{O}$ oliv	$^{3}\text{He}/^{4}\text{He}^c$	^{4}He cc	Olivine mass (g)	Fraction He blank
	2 σ	2 σ	2 σ	2 σ		1 σ	STP/g		
DB-17	15.2942	0.0037	37.455	0.009	0.87341	0.00002	2.13882	0.00007	5.17
DB-17 fusion									7.53E-11
DB-19	15.3929	0.0009	37.971	0.003	0.85472	0.00002	2.10846	0.00005	6.4
PI-10	15.4001	0.0035	37.920	0.011	0.85735	0.00003	2.11085	0.00004	0.2
PI-15	15.4223	0.0025	37.723	0.008	0.85980	0.00002	2.10296	0.00006	0.4
PI-17	15.3663	0.0012	37.662	0.002	0.86545	0.00001	2.12113	0.00015	0.5
PI-18	15.3680	0.0011	37.660	0.003	0.86560	0.00002	2.12116	0.00004	0.6
PI-20	15.3642	0.0015	37.659	0.004	0.86540	0.00002	2.12107	0.00007	0.7
BCR-2 ^e									0.20028
BCR-2 ^e									0.18434
BCR-2 ^{e,f}									0.19551
AGV-2 ^f									0.50
AGV-2 ^f									0.42
BCR-2 ^f									0.05
AGV-2 ^f									0.05
BCR-2 ^g	15.6251	0.0008	38.7414	0.0022					0.11
AGV-2 ^g	15.6174	0.0009	38.5299	0.0032					0.15

^aFor the 11 samples with available pillow glass, heavy radiogenic isotopes were measured on glass; for the remaining samples they were measured on rock chips. ^b ^{143}Nd is calculated assuming a chondritic value from Bouvier et al. (2008). ^cWith three exceptions, all of the helium isotopic analyses were made following crushing olivines in vacuo. Using the crushed powders remaining for the $^{3}\text{He}/^{4}\text{He}$ crush analyses, three fusion experiments were conducted here, on samples DB-17, AK-8b, and AK-9.

^dFor AK-13, the 28.8 R_A olivine crush values is for a single megacryst (73 mg) and the 21.5 R_A replicate value is from 137 mg of smaller olivine crystals.

^eAn aliquot of the USGS reference material BCR-2 was run with each analytical session for Nd isotopic analyses. ^fHf and Pb isotopic compositions of the USGS reference materials BCR-2 and AGV-2 shown here were reported in Price et al. (2016) and were run in separate analytical sessions from the samples in this study, but in the same laboratory (Lyon) following exactly the same procedures (described in Price et al., 2016).

Table 3
Oxygen Isotopic Compositions of Baffin Island Olivines

Sample ID	Mass (mg)	$\delta^{18}\text{O}$	1σ	$\mu\text{mol O}_2$	$\mu\text{mols O}_2/\text{mg}$
AK-1	1.48	5.24	0.07	19.11	12.54
AK-1-replicate	1.43	5.19	0.07	18.79	12.76
sample average		5.21			
AK-6	1.05	5.38	0.07	14.24	13.56
AK-6-replicate	1.20	5.27	0.07	15.38	12.82
AK-6-rep2	0.70	5.35	0.07	9.1	13.00
sample average		5.33			
AK-8b	1.36	5.08	0.07	18.86	13.87
AK-8b-replicate	1.67	4.98	0.07	23.18	13.88
sample average		5.03			
AK-13	1.29	5.24	0.07	17.28	13.40
AK-13-replicate	0.86	5.40	0.10	11.1	12.98
sample average		5.32			
AK-14	0.90	5.12	0.07	11.27	12.16
DB-9	1.32	5.06	0.07	17.45	13.22
DB-9-replicate	1.18	5.14	0.07	15.12	12.81
sample average		5.10			
DB-13	1.40	5.03	0.07	18.36	12.73
DB-14	1.22	5.10	0.07	16.31	13.37
DB-14-replicate	1.25	5.09	0.07	16.77	13.42
sample average		5.09			
DB-17	1.33	5.16	0.07	16.03	12.05
DB-17-replicate	1.21	5.18	0.07	16.78	13.87
sample average		5.17			
DB-19	1.19	5.02	0.07	15.77	13.25
DB-19-replicate	1.23	5.13	0.07	16.29	13.24
sample average		5.08			
PI-15	1.32	5.12	0.07	18.09	13.70
PI-15-replicate	1.27	5.31	0.07	16.72	13.17
sample average		5.21			
PI-18	1.35	5.17	0.07	18.55	13.74
PI-18-replicate	1.25	5.19	0.07	17.36	13.89
sample average		5.18			
PI-20	1.47	4.89	0.07	20.12	13.29
PI-20-replicate	1.64	5.17	0.07	22.23	13.16
PI-20-replicate	1.29	5.15	0.07	17.9	13.88
sample average		5.07			

(~12; Hofmann & White, 1983) and Rb/Cs (85–95; Hofmann & White, 1983) ratios of fresh basalts. In the new suite of Baffin Island lavas, Ba/Rb and Rb/Cs vary from 5.8–69.0 and 42–424, respectively (Table 1).

As previously noted, large degrees of crustal assimilation are associated with low MgO, Nb/Th, and Ce/Pb in mantle-derived lavas erupted in continental settings. In Figure 6, West Greenland basement samples (compiled in Larsen & Pedersen, 2009) are shown together with Baffin Island–West Greenland lavas. At lower Nb/Th and Ce/Pb, a subset of Baffin Island–West Greenland lavas trend away from MORB-like compositions toward compositions identified in the basement.

3.4. Sr-Nd-Hf-Pb Isotopic Compositions

Measured Sr, Nd, and Hf isotopic compositions of the 18 Baffin Island lavas in this data set range from 0.702995 to 0.703946 for $^{87}\text{Sr}/^{86}\text{Sr}$, 0.512920 to 0.513174 for $^{143}\text{Nd}/^{144}\text{Nd}$, and 0.283144 to 0.283287 for $^{176}\text{Hf}/^{177}\text{Hf}$. The ranges for Pb isotopes span 17.5114 to 18.0095, 15.2887 to 15.4291, and 37.455 to 37.971 for $^{206}\text{Pb}/^{204}\text{Pb}$, $^{207}\text{Pb}/^{204}\text{Pb}$, and $^{208}\text{Pb}/^{204}\text{Pb}$, respectively (Table 2).

Figure 7 shows that some Baffin Island–West Greenland lavas with low Nb/Th, Ce/Pb, and MgO also have relatively high $^{87}\text{Sr}/^{86}\text{Sr}$ and low $^{143}\text{Nd}/^{144}\text{Nd}$, in some cases approaching radiogenic isotopic values observed in the basement, which has highly geochemically enriched $^{87}\text{Sr}/^{86}\text{Sr}$ (0.713758 to 0.823010) and $^{143}\text{Nd}/^{144}\text{Nd}$ (0.510737 to 0.511945; Figure 7). Most basement samples extend to lower $^{206}\text{Pb}/^{204}\text{Pb}$ than those found in MORB, and Baffin Island–West Greenland lavas with the lowest Nb/Th, Ce/Pb, and MgO also tend to have low $^{206}\text{Pb}/^{204}\text{Pb}$ and extend to the unradiogenic values identified in the basement.

After applying the filters for crustal contamination, only four lavas from the Baffin Island–West Greenland suite—AK-8b, DB-13, DB-14, and PI-15—with modern high-precision Sr, Nd, Hf, and Pb isotopic data can be considered “least crustally contaminated” (see Table 2). (We note that an additional five West Greenland lavas fall in this category as well but lack Hf and Pb isotopic compositions determined with modern methods; Larsen & Pedersen, 2009). While it is unfortunate that so few lavas can be considered (near) primary, it is preferable to focus only on those lavas that best reflect the composition of the mantle source.

The four Baffin Island lavas with mantle-like Nb/Th, Ce/Pb, and high-precision Sr, Nd, Hf, and Pb isotopic data, all from this study, plot in the geochemically depleted region of the $^{143}\text{Nd}/^{144}\text{Nd}$ versus $^{87}\text{Sr}/^{86}\text{Sr}$ and $^{176}\text{Hf}/^{177}\text{Hf}$ versus $^{143}\text{Nd}/^{144}\text{Nd}$ plots (Figure 8, right panels).

In order to compare the Baffin Island samples with MORB and younger lavas associated with the Iceland plume, we focus on the isotopic compositions calculated for the Baffin Island mantle today (which overlap the measured isotopic ratios), because the age-corrected data are less appropriate for comparison with the significantly younger high- $^3\text{He}/^4\text{He}$ lavas from Iceland (all of which are stratigraphically younger than 14.9 Ma; Hardarson et al., 1997; McDougall et al., 1984). In section S2.3 of the supporting information, we provide a method for constraining the present-day composition of the Baffin Island mantle source (i.e., the composition of the source if it had not experienced melt extraction at 60 Ma) to avoid having to compare age-corrected Sr, Nd, Hf, and Pb isotopic compositions in Baffin Island lavas with measured compositions in much younger MORB and Iceland lavas (calculated present-day compositions for Baffin Island lavas are shown in Figures 8, 9, and 12). The four least crustally contaminated Baffin Island lavas with mantle-like Nb/Th and Ce/Pb plot within the field for global MORB located far from hotspots in all radiogenic isotopic spaces (Figures 8 and 9). However, in plots that include $^{206}\text{Pb}/^{204}\text{Pb}$, they are offset from the field for North

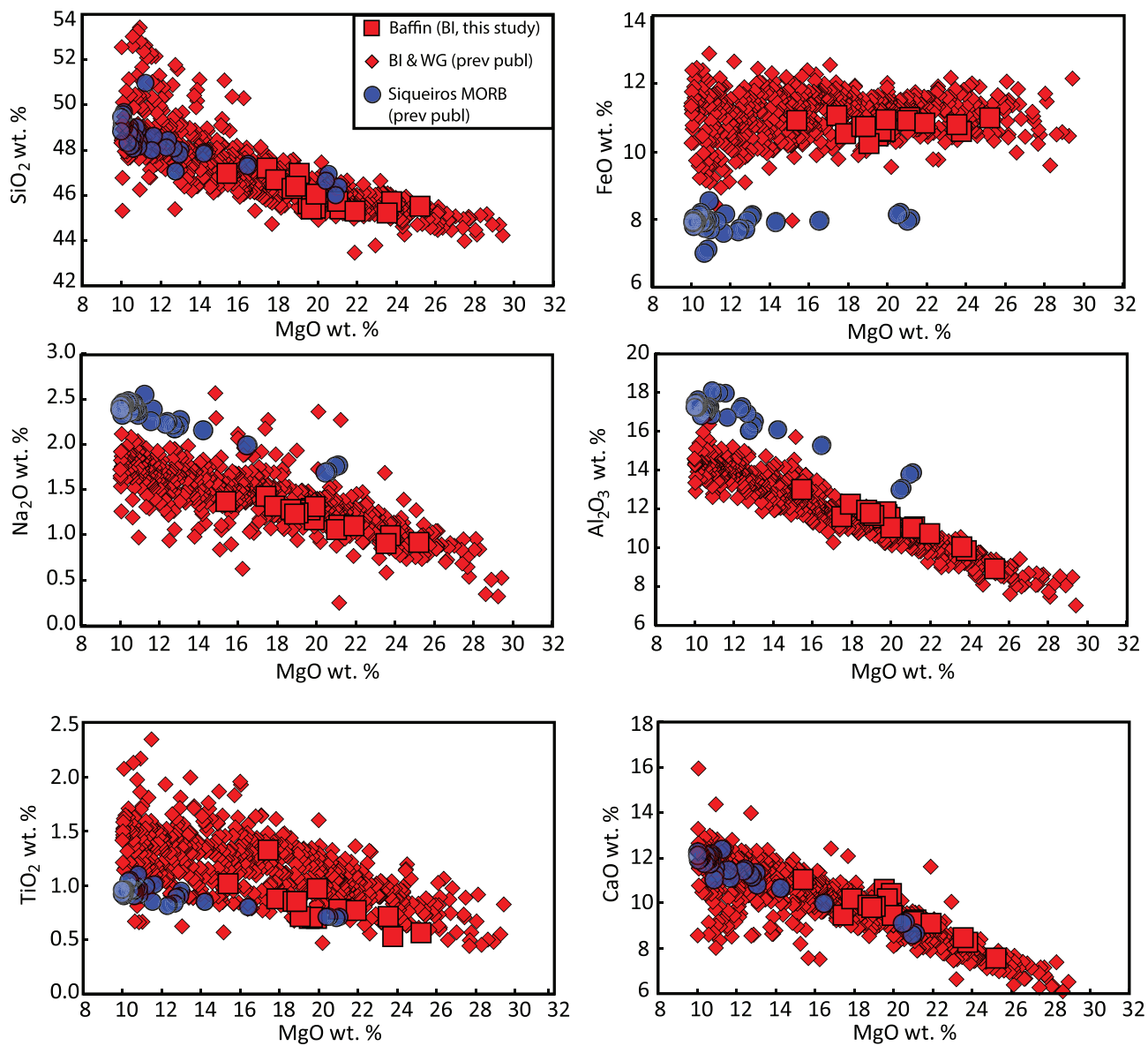


Figure 2. Major element compositions of Baffin Island (BI) lavas from this study (red squares) and other sources (red diamonds; Francis, 1985; Jackson et al., 2010; Starkey et al., 2009; Stuart et al., 2003; Yaxley et al., 2004). Also shown are West Greenland (WG) lavas (also red diamonds) compiled in Larsen and Pedersen (2009). Baffin Island and West Greenland lavas are not filtered for crustal assimilation; however, only lavas with MgO > 10 wt.% are shown. High-MgO (> 10 wt.%) Siqueiros MORB samples compiled in Hays (2004) and Perfit et al. (1996) are shown for comparison. Major element compositions for Baffin Island and West Greenland differ systematically from MORB such that, for example, the flood basalt lavas have higher FeO at a given MgO. These important petrologic differences are interpreted to be the result of deeper melting and higher melt fraction in the hotter plume setting.

Atlantic MORB (i.e., MORB samples located between 50 and 80°N that are >500 km away from hotspots), but overlap with it in plots of $^{143}\text{Nd}/^{144}\text{Nd}$ versus $^{87}\text{Sr}/^{86}\text{Sr}$ and $^{176}\text{Hf}/^{177}\text{Hf}$ versus $^{143}\text{Nd}/^{144}\text{Nd}$ (Figure 9). The radiogenic isotopic compositions of the four least contaminated Baffin Island lavas do not consistently overlap with the field for mid-Miocene to modern (neovolcanic zone) Iceland lavas, but partially overlap with the geochemically depleted (Sr, Nd, and Hf) and unradiogenic (Pb) portion of the modern (neovolcanic zone) Iceland field. Additionally, they fall on or close to the 4.5 Ga geochron (Figure 9), an observation consistent with that made by Jackson et al. (2010).

3.5. Oxygen Isotopic Compositions

In Figure 10, the oxygen isotopic compositions measured on Baffin Island olivines from this study are shown together with previously published olivine oxygen isotopic data (Kent et al., 2004). The oxygen isotopic data

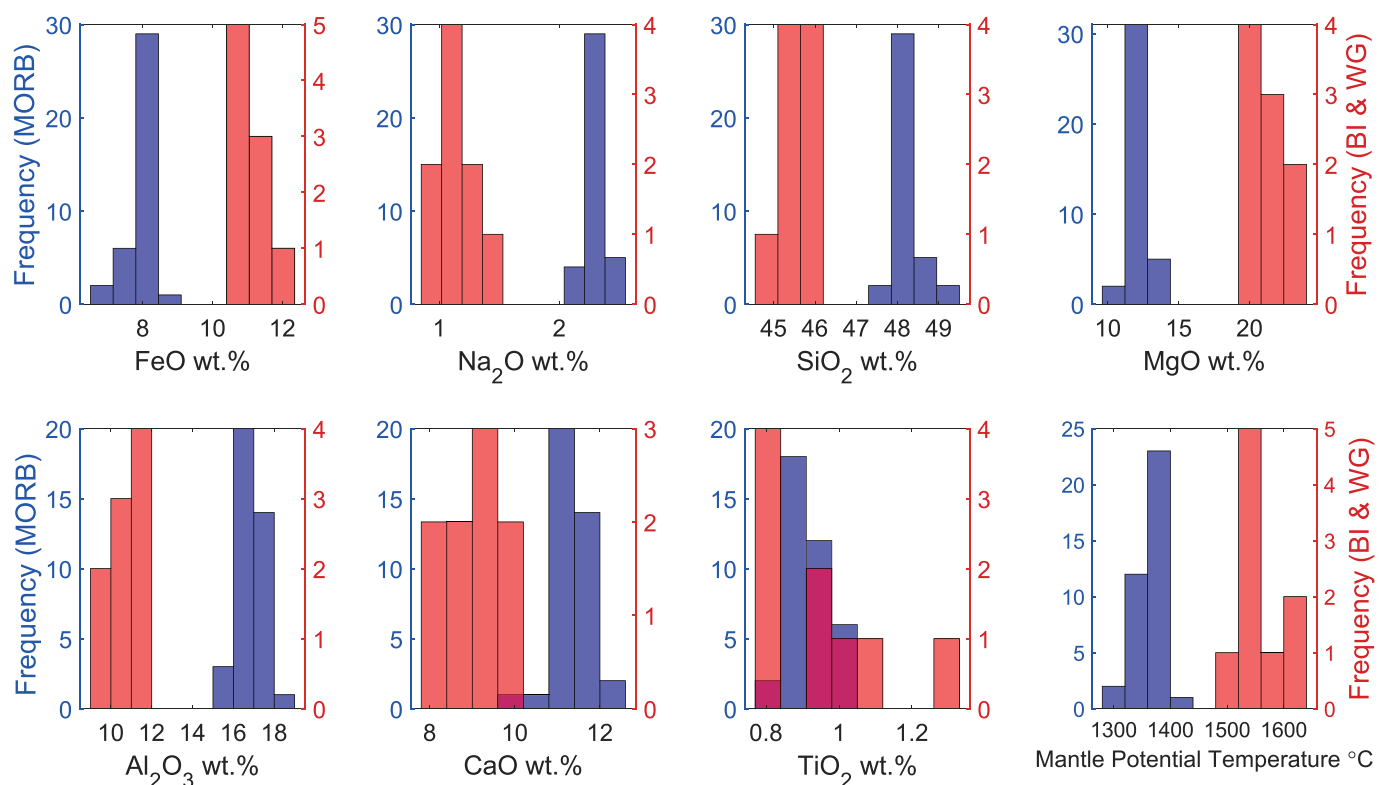


Figure 3. Histogram of calculated primary melt compositions for high-MgO (>10 wt.%) Siqueiros MORB (blue) from the Siqueiros transform fault from Perfit et al. (1996) and Hays (2004) and primary melt compositions for Baffin Island (BI) and West Greenland (WG) lavas (red). The data in the histograms are consistent with hotter, deeper melting at BI-WG compared to MORB. BI-WG samples have been filtered for crustal assimilation so that all lavas plotted have Nb/Th > 13, Ce/Pb > 20, and MgO > 10 wt.%; high-Ba/Th (>100) samples from West Greenland are not considered as they are deemed modified by mantle metasomatism. Primary melts are calculated using PRIMELT3 from Herzberg and Asimow (2015) using Fe₂O₃/TiO₂ = 0.5 and accumulated fractional melting. Mantle potential temperatures calculated with PRIMELT3 software are also shown. The number of samples for BI-WG ($N = 9$) is greater here than in the isotope plots because isotopes are not required for petrologic analyses.

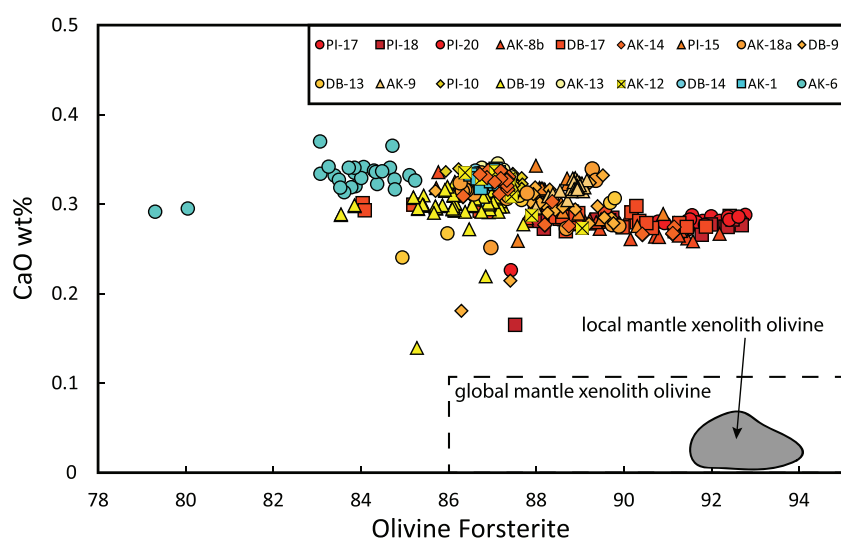


Figure 4. Olivine CaO composition compared to forsterite content of olivines in all 18 samples examined in this study. Color coding reflects maximum forsterite content: Red reflects samples with highest maximum forsterite. The CaO at a given forsterite value is distinctly higher in Baffin Island lava olivines compared to olivines found in global mantle xenoliths (from Hervig et al., 1986) and local mantle xenoliths from Ubekendt Ejland, West Greenland (Bernstein et al., 2006). Higher CaO in the picrite olivines demonstrates that these olivines were not mechanically entrained from the lithospheric mantle during magma ascent.

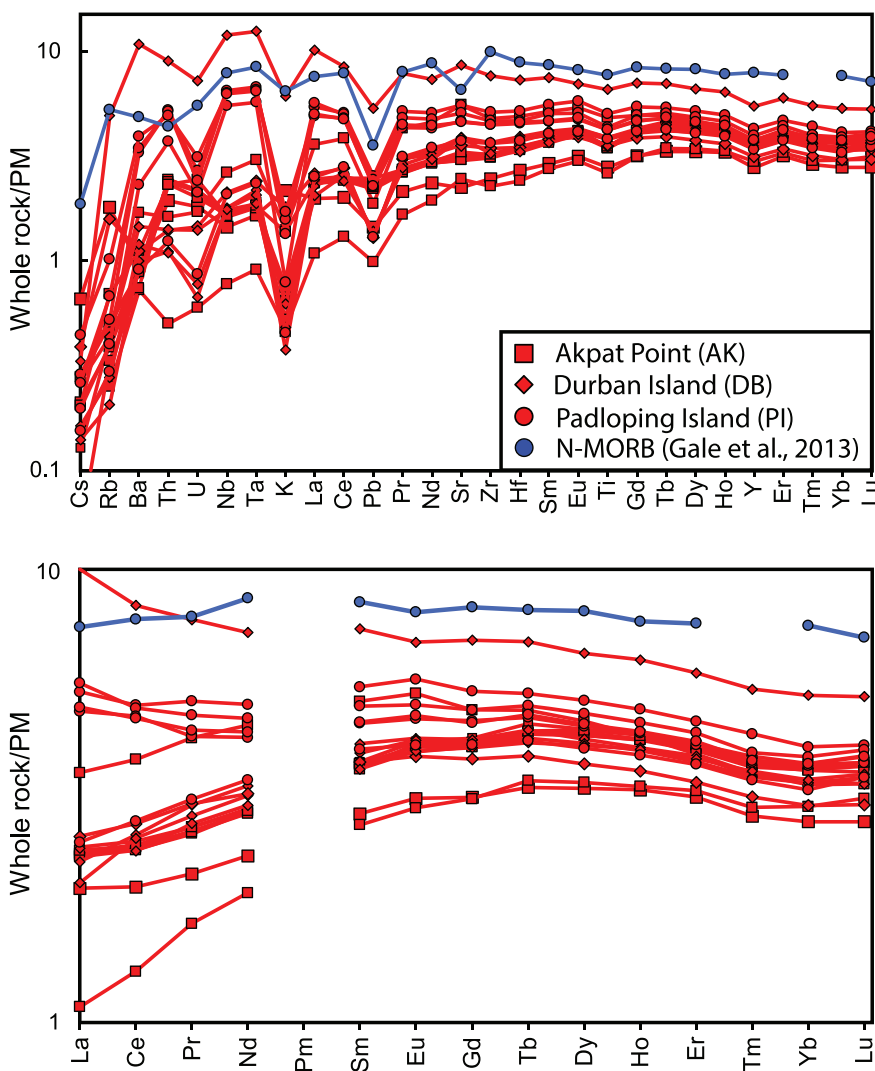


Figure 5. Primitive mantle (McDonough & Sun, 1995) normalized trace element patterns for Baffin Island lavas examined in this study plotted with an average N-MORB composition from Gale et al. (2013; using the MORB average that excludes back arc basins and lavas located <500 km from known hotspots). For elements that have both XRF and ICP-MS data are plotted here.

are compared with olivine forsterite content and basalt Nb/Th. The four least crustally contaminated Baffin Island lavas have olivine $\delta^{18}\text{O}$ indistinguishable from MORB olivines (5.0–5.2 ‰; Eiler, 2001), and olivines from all lavas in this study fall within the range defined by mantle olivine $\delta^{18}\text{O}$ from Mattey et al. (1994) (5.18 \pm 0.28 ‰). However, at low olivine forsterite and low basalt Nb/Th (associated with crustal assimilation), olivine $\delta^{18}\text{O}$ values in some of the Baffin Island lavas plot outside of the window defined by MORB olivines.

3.6. Helium Concentrations and Isotopic Compositions

Figure 11 summarizes the helium results for olivine *in vacuo* crushing determinations for Baffin Island-West Greenland lavas from this and previous studies (Graham et al., 1998; Jackson et al., 2010; Stuart et al., 2003; Starkey et al., 2009 and Rizo et al., 2016). Olivine crushing in vacuo is the most common helium extraction method because it primarily releases gas from fluid and melt inclusions, which is the best determination of magmatic helium isotopic compositions, due to the possible presence of cosmogenic and/or radiogenic helium in the olivine matrix. Figure 11 demonstrates that helium concentrations are highly variable in the Baffin Island olivines (a factor of 370), most likely reflecting variable abundances of trapped melt and fluid inclusions in the olivines. The olivine crush experiments for the samples in this study yield ${}^3\text{He}/{}^4\text{He}$

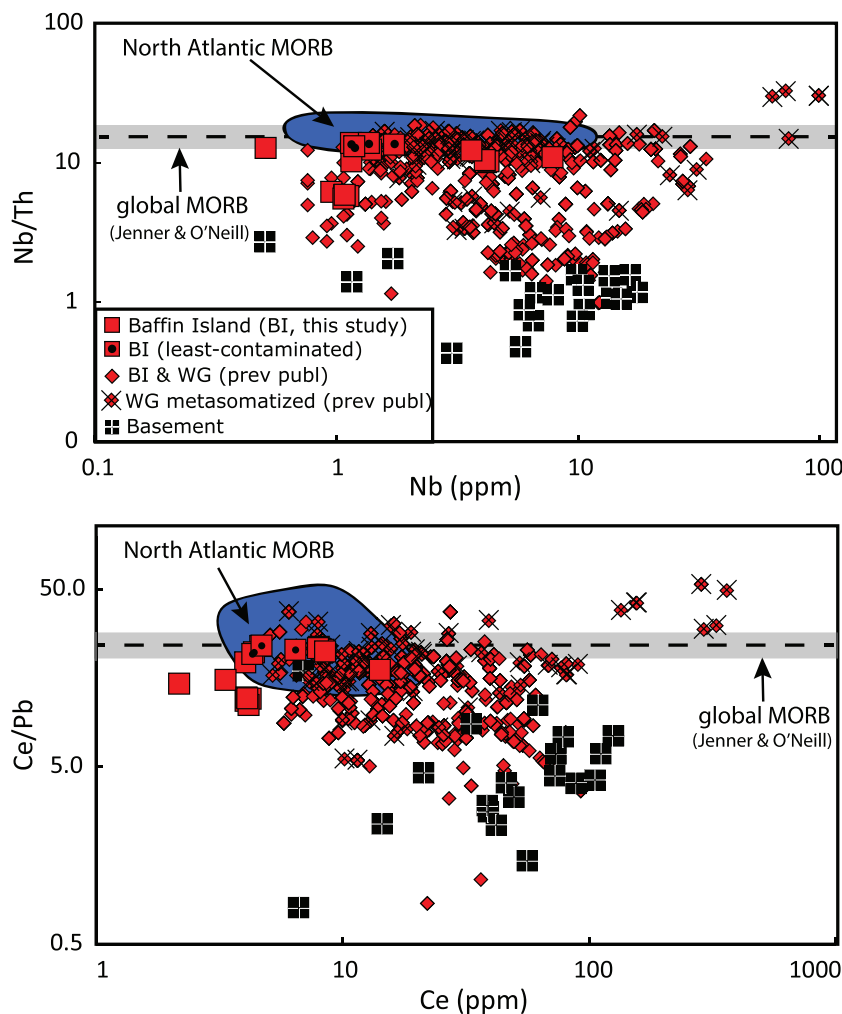


Figure 6. Nb/Th and Ce/Pb plotted against (top) Nb and (bottom) Ce concentrations, respectively. The least contaminated lavas from this study ($N = 4$) are denoted by a small black circle within the red square symbol. Continental crust rocks from West Greenland (WG; Larsen & Pedersen, 2009) have low Nb/Th and Ce/Pb . Low Nb/Th and Ce/Pb in Baffin Island and West Greenland lavas therefore are associated with higher degrees of continental crust assimilation. Baffin Island (BI) and West Greenland samples considered to be crustally contaminated have $\text{Nb}/\text{Th} < 13$ and/or $\text{Ce}/\text{Pb} < 20$ (and/or $\text{MgO} < 10$ wt.%, not shown). These threshold values are the lower limit of the “mantle composition” defined by the MORB database of Jenner and O’Neill (2012), which is shown as a dashed line and gray field (± 1 SD) in both panels. Baffin Island and West Greenland lavas from a metasomatized source ($\text{Ba}/\text{Th} > 100$) are marked with a black “X” over the red diamonds. The North Atlantic MORB field is from Gale et al. (2013) and includes only MORB samples from 50 to 80°N that are >500 km from known hotspots (using the hotspot database of King & Adam, 2014).

ranging from 0.17 to $56.6 R_A$, encompassing known values for terrestrial, mantle-derived rocks. In general, Baffin Island-West Greenland olivine samples with low ${}^4\text{He}$ concentrations ($< 1.0 \times 10^{-9} \text{ cc STP/g}$) have lower ${}^3\text{He}/{}^4\text{He}$, due to greater potential for atmospheric contamination in low- ${}^4\text{He}$ samples, and greater sensitivity to reduction in ${}^3\text{He}/{}^4\text{He}$ by posteruptive radiogenic ingrowth of ${}^4\text{He}$ (Hilton et al., 1995). Two samples—AK-9 and DB-17—plot above the trend defined by Baffin Island-West Greenland lavas in ${}^3\text{He}/{}^4\text{He}$ versus ${}^4\text{He}$ space, and, given their low ${}^4\text{He}$ concentrations, were selected for fusion experiments (together with AK-8b) on crushed powders to test for cosmogenic ${}^3\text{He}$ influence.

Basaltic olivines with cosmogenic helium typically yield magmatic helium via crushing and extremely high ${}^3\text{He}/{}^4\text{He}$ from fusion, reflecting spallation ${}^3\text{He}$ in the solid olivine (e.g., Kurz, 1986). Sample AK-9, which has the highest ${}^3\text{He}/{}^4\text{He}$ crush experiment in this study (AK-9, $56.6 \pm 1.1 R_A$), yielded a ${}^3\text{He}/{}^4\text{He}$ of $36.3 R_A$ and ${}^4\text{He}$ concentration of $5.2 \times 10^{-9} \text{ cc STP/g}$ by fusion of the powder remaining after crushing. The ${}^3\text{He}/{}^4\text{He}$ from the crush experiment of AK-9 is treated with caution due to the low ${}^4\text{He}$ concentration (1.4×10^{-10}

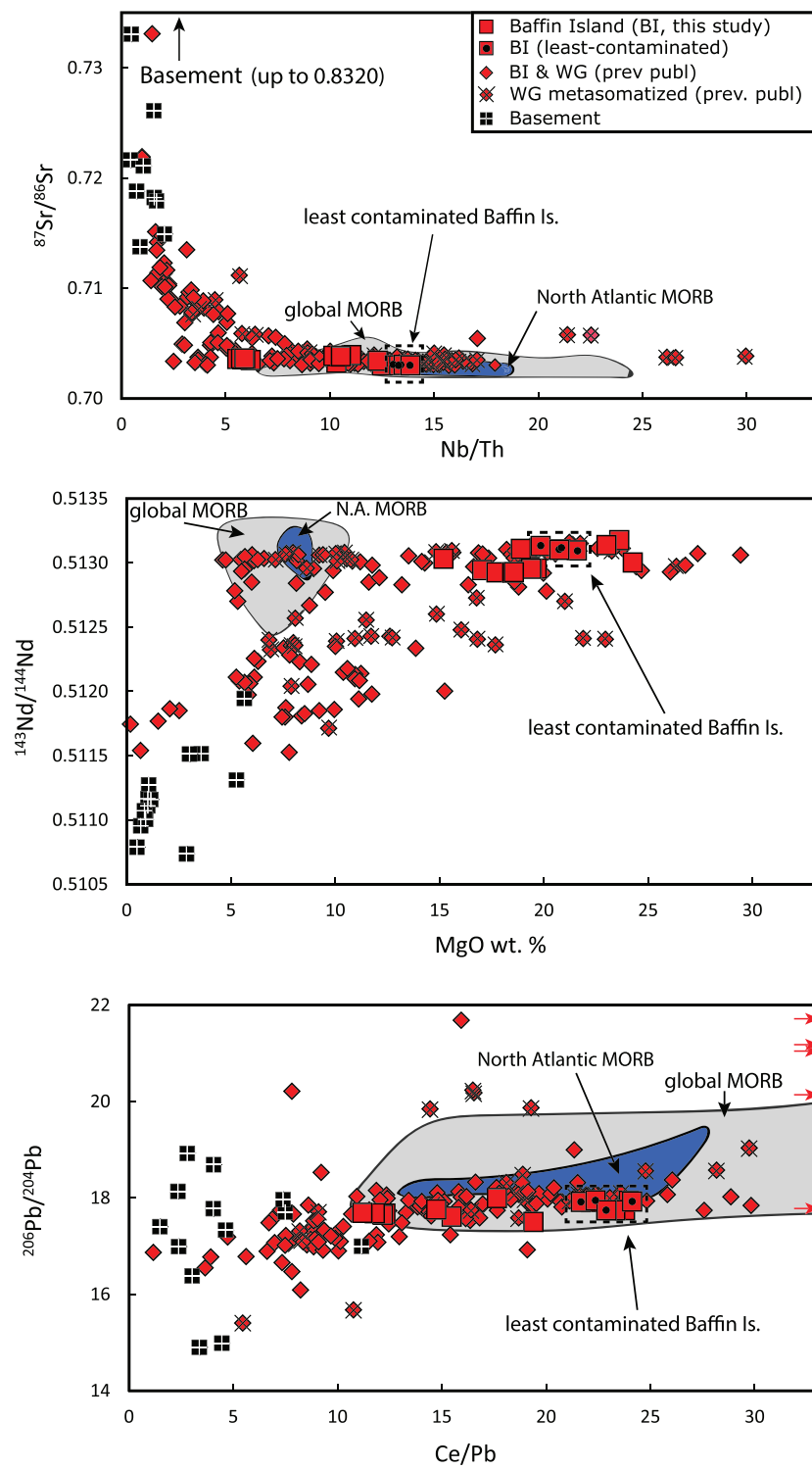


Figure 7. Sr, Nd, and Pb isotope compositions of Baffin Island (BI) and West Greenland (WG) lavas plotted as a function of the three geochemical indicators for crustal assimilation used here: Nb/Th, MgO, and Ce/Pb. All isotopic data plotted are measured data. Greater degrees of crustal assimilation are associated with lower Nb/Th, Ce/Pb, and MgO; Baffin Island and West Greenland lavas with evidence for crustal contamination also have higher $^{87}\text{Sr}/^{86}\text{Sr}$, lower $^{143}\text{Nd}/^{144}\text{Nd}$, and generally lower $^{206}\text{Pb}/^{204}\text{Pb}$. Lavas ($N = 4$) identified as the least crustally contaminated using these criteria are marked with a black dot within the red square and outlined with a dashed box. Baffin Island and West Greenland lavas from a metasomatized source ($\text{Ba/Th} > 100$) are marked with a black "X" over the red diamonds. In the bottom panel, five samples (shown with red arrows) with $\text{Ba/Th} > 100$ plot outside the panel. The North Atlantic (50 to 80°N) and global MORB fields are from Gale et al. (2013) and include only MORB samples located >500 km from known hotspots (using the hotspot database of King & Adam, 2014).

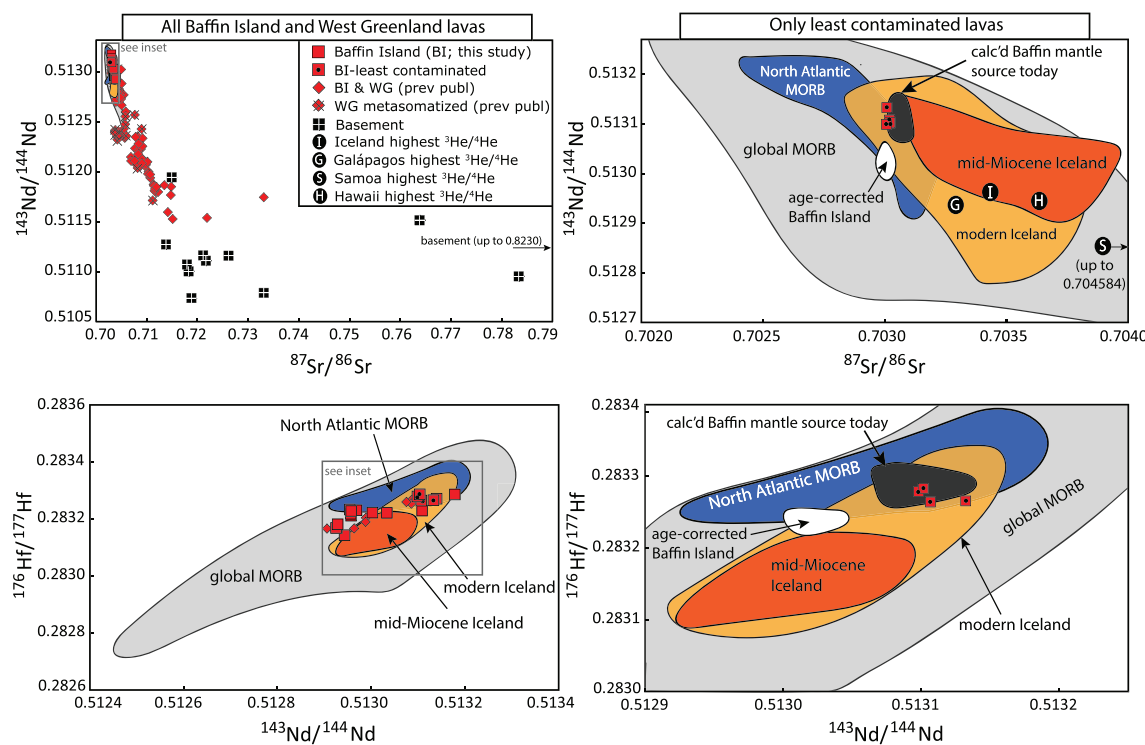


Figure 8. Sr, Nd, and Hf isotopic compositions of Baffin Island (BI) lavas from this study (red squares) shown together with previously published data from Baffin Island and West Greenland (WG; both as red diamonds; Jackson et al., 2010; Starkey et al., 2009; Larsen & Pedersen, 2009; Kent et al., 2004, and references therein). Data points shown are the measured isotopic compositions and white and dark gray fields reflect age-corrected and calculated present-day mantle source compositions, respectively (see section S2.3 and Figure S2 in the supporting information). Age correction of the mid-Miocene and modern Iceland lavas is negligible (offset is less than the size of the Baffin Island lava symbols; Figure S3) and the respective fields represent measured data. All isotopic data plotted as symbols here are measured data. Age-corrected data and calculated present-day mantle compositions, are shown as fields in the right-hand side panels. Both crustally contaminated and least crustally contaminated Baffin Island-West Greenland lavas are shown in the left-hand side panels, whereas only the least crustally contaminated lavas ($\text{Nb}/\text{Th} > 13$, $\text{Ce}/\text{Pb} > 20$, MgO wt.% > 10) are shown in the right-hand side panels. Paired Hf and Nd isotopic compositions are available from only two studies—this study (red squares) and Jackson et al. (2010; red diamonds), explaining the smaller data set available for plotting. Mid-Miocene Iceland (darker orange field), modern Iceland (lighter orange field), North Atlantic MORB (50 to 80°N; blue field), and global MORB (light gray field) fields are shown for perspective (Iceland data from GEOROC, <http://georoc.mpch-mainz.gwdg.de/georoc/>; MORB data from Gale et al., 2013); MORB fields exclude back-arc basin lavas and MORB samples <500 km from nearby hotspots (King & Adam, 2014). Lavas with the highest ${}^3\text{He}/{}^4\text{He}$ compositions from Iceland, Galápagos, Hawaii, and Samoa are indicated by the black circles with the letters I, G, H, and S, respectively (see Jackson et al., 2008).

cc STP/g) and high (43%) contribution from blank. Another sample with coupled crush/fusion measurements, DB-17, has a crushed ${}^3\text{He}/{}^4\text{He}$ of $31.2 \pm 0.9 R_A$ (${}^4\text{He} = 7.5 \times 10^{-11}$ cc STP/g) and a fusion ${}^3\text{He}/{}^4\text{He}$ of $6.4 R_A$ (${}^4\text{He} = 4.7 \times 10^{-9}$ cc STP/g). Critically, the high ${}^3\text{He}/{}^4\text{He}$ value ($39.9 \pm 0.5 R_A$) for an olivine crush experiment, determined in sample AK-8b, has the highest ${}^4\text{He}$ concentration (2.3×10^{-8} cc STP/g) and plots within the field of data populated by previously published high- ${}^3\text{He}/{}^4\text{He}$ lavas in the ${}^3\text{He}/{}^4\text{He}$ versus ${}^4\text{He}$ (cc STP/g) plot and is considered the most robust high- ${}^3\text{He}/{}^4\text{He}$ measurement in this study. A fusion experiment on the AK-8b crushed olivine powder yielded ${}^3\text{He}/{}^4\text{He}$ of $20.8 R_A$ (and ${}^4\text{He} = 1.84 \times 10^{-8}$ cc STP/g). In *all three* samples with paired crushed-powder fusions, the fusion measurements yielded *lower* ${}^3\text{He}/{}^4\text{He}$ than crushing, suggesting that radiogenic helium is a significant contribution. These data demonstrate that cosmogenic helium does not dominate in the olivines and is not a likely contributor to the crushing experiments, because if that were the case one would expect cosmogenic helium to have *higher* ${}^3\text{He}/{}^4\text{He}$. The lack of high ${}^3\text{He}/{}^4\text{He}$ in the fusion measurements does not exclude the possibility of small amounts of cosmogenic helium, but strongly suggests it is not a contribution to the crushing measurements. Olivine typically has extremely low Th and U abundances (ppb), but radiogenic helium can be implanted into the olivine crystal surfaces from the solid matrix (which has ppm levels of Th and U), which is released by fusion and not by crushing (e.g., Jackson et al., 2010; Moreira et al., 2012). The comparison between a megacryst and smaller grain size olivines from the same sample

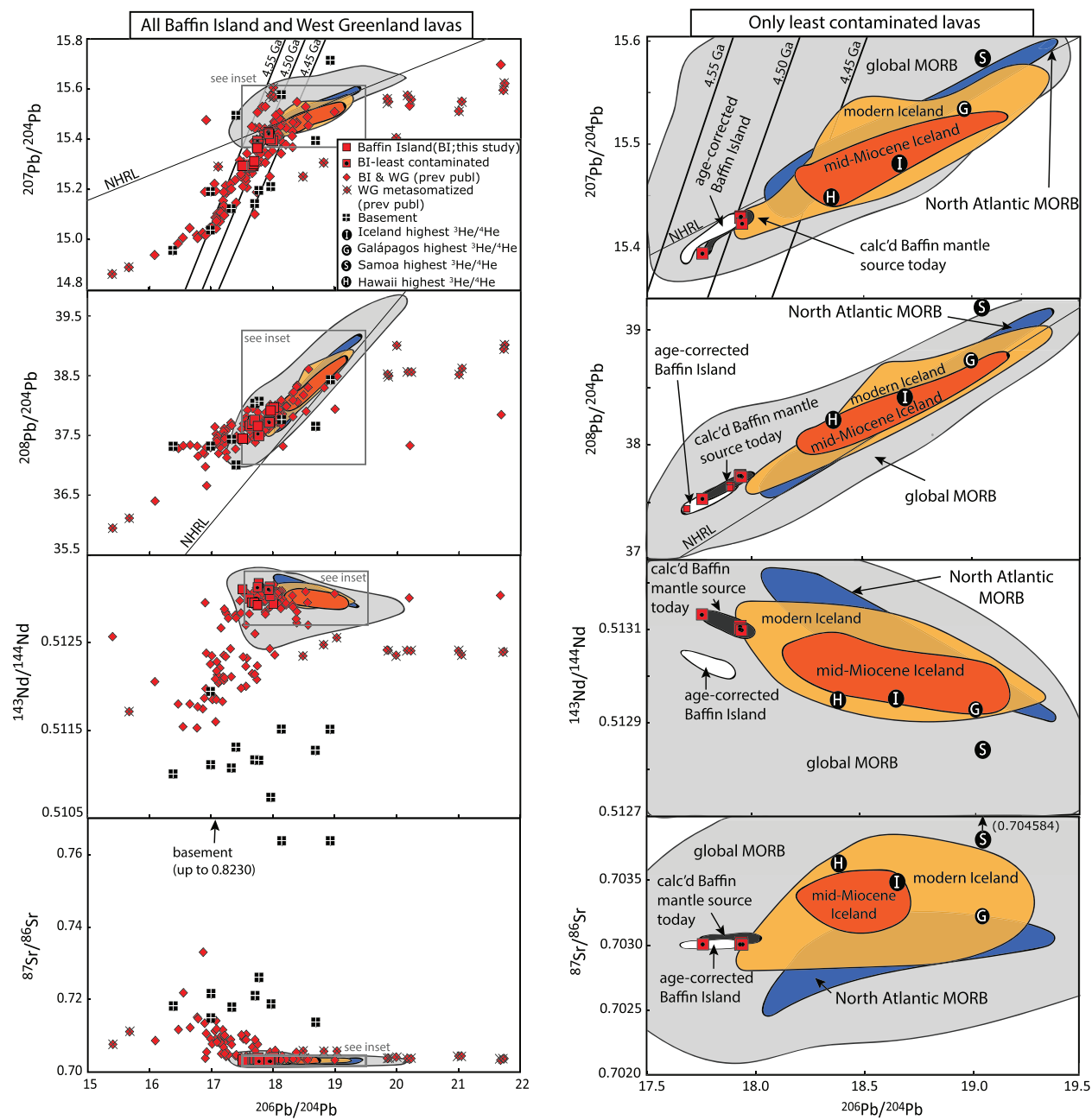


Figure 9. Sr, Nd, and Pb isotopic compositions of Baffin Island (BI) lavas from this study (red squares) shown together with previously published data from Baffin Island and West Greenland (WG; both red diamonds; Jackson et al., 2010; Starkey et al., 2009; Larsen & Pedersen, 2009; Kent et al., 2004, and references therein). Data points shown are the measured isotopic compositions, while white and dark gray fields reflect age-corrected and calculated present-day mantle source compositions, respectively (see section S2.3 and Figure S2 in the supporting information). Age correction of the mid-Miocene and modern Iceland lavas is negligible (offset is less than the size of the Baffin Island lava symbols; Figure S3) and the respective fields represent measured isotopic ratios. Crustally contaminated and least crustally contaminated Baffin Island-West Greenland lavas are shown in the left-hand side panels, whereas only the least crustally contaminated lavas ($\text{Nb}/\text{Th} > 13$, $\text{Ce}/\text{Pb} > 20$, MgO wt.% > 10) are shown in the right-hand side panels. Mid-Miocene Iceland (darker orange field), modern Iceland (lighter orange field), and North Atlantic MORB (50 to 80°N) (blue field) and global MORB (light gray field) fields are shown for perspective (Iceland data from GEOROC, <http://georoc.mpch-mainz.gwdg.de/georoc/>; MORB data from Gale et al., 2013); MORB fields exclude back-arc basin lavas and MORB samples <500 km from nearby hotspots (King & Adam, 2014). For all plots that include Pb isotopes, fields for mid-Miocene and modern Iceland are defined using high-precision MC-ICP-MS data only, while MORB fields also include unspiked Pb isotopic data acquired by TIMS. For Pb isotopic data obtained on Baffin Island and West Greenland, both MC-ICP-MS and unspiked TIMS Pb isotopic data are included in the “global plots” (i.e., left-hand side panels), whereas only samples with MC-ICP-MS Pb isotopic data are shown in the right-hand side panels. In the Sr-Pb panel, mid-Miocene Iceland has a narrower range than other panels because the highest and lowest $^{206}\text{Pb}/^{204}\text{Pb}$ samples lack Sr isotopic analyses. Lavas with the highest $^3\text{He}/^4\text{He}$ compositions from Iceland, Galápagos, Hawaii, and Samoa are indicated by the black circles with the letters I, G, H, and S, respectively (see Jackson et al., 2008).

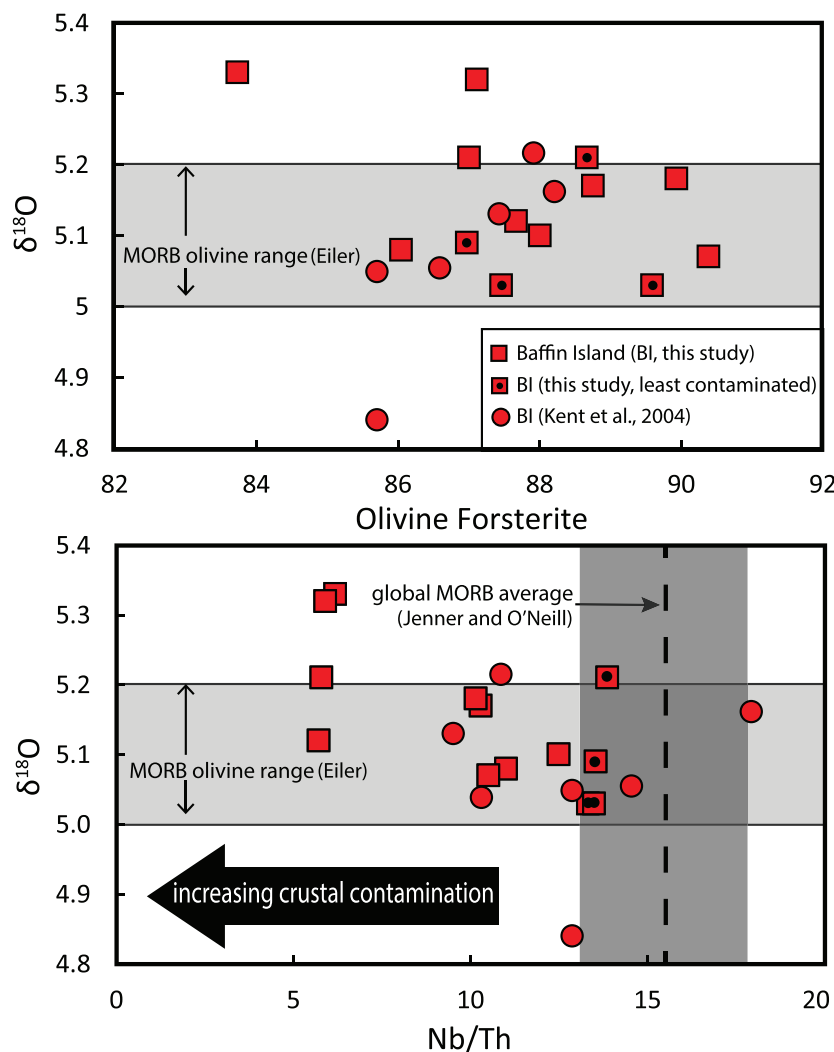


Figure 10. $\delta^{18}\text{O}$ compositions of Baffin Island olivines from this study (red squares) and Kent et al. (2004; red circles) compared with olivine forsterite and Nb/Th. The range of $\delta^{18}\text{O}$ in MORB olivine (light gray bar) is from Eiler (2001). The range of Nb/Th in MORB is from Jenner and O'Neill (2012) and includes 1σ variation (dark gray bar). Low Nb/Th, which is associated with higher degrees of crustal assimilation, may relate to somewhat higher $\delta^{18}\text{O}$. The four Baffin Island lavas that are “least crustally contaminated” (based on having high mantle-like Nb/Th, Ce/Pb, and MgO) also have MORB-like $\delta^{18}\text{O}$.

(AK-13) supports the importance of ^4He implantation from the groundmass, that is, with greater effect on smaller crystals with fewer melt inclusions.

When focusing only on Baffin Island samples with mantle-like Nb/Th and Ce/Pb (i.e., least crustally contaminated), paired $^3\text{He}/^4\text{He}$ and Sr-Nd-Pb isotopic measurements show that the least contaminated Baffin Island lavas have a distinct radiogenic isotopic composition from the highest observed $^3\text{He}/^4\text{He}$ lavas from Iceland, Galápagos, Hawaii, and Samoa (marked as “I,” “G,” “H,” and “S” in Figures 8 and 9). For example, while the upper envelope of $^3\text{He}/^4\text{He}$ in Icelandic lavas increases with increasing $^{87}\text{Sr}/^{86}\text{Sr}$ —where the highest $^3\text{He}/^4\text{He}$ of $37.7 R_A$ is at 0.703465 —the measured $^{87}\text{Sr}/^{86}\text{Sr}$ of the least contaminated Baffin Island lavas defines a narrow range of lower values (0.703008 – 0.703021) at all $^3\text{He}/^4\text{He}$ values (0.703009 at $39.9 R_A$; Figure 12). Thus, the Iceland data form a trend that diverges away from the Baffin Island lavas, and this observation holds for both the measured $^{87}\text{Sr}/^{86}\text{Sr}$ ratio and the calculated present-day $^{87}\text{Sr}/^{86}\text{Sr}$ for the Baffin Island mantle source. Similarly, a plot of $^3\text{He}/^4\text{He}$ versus $^{143}\text{Nd}/^{144}\text{Nd}$ shows that the highest $^3\text{He}/^4\text{He}$ Iceland lavas have lower $^{143}\text{Nd}/^{144}\text{Nd}$ (0.512969) than the measured $^{143}\text{Nd}/^{144}\text{Nd}$ (0.513128) and

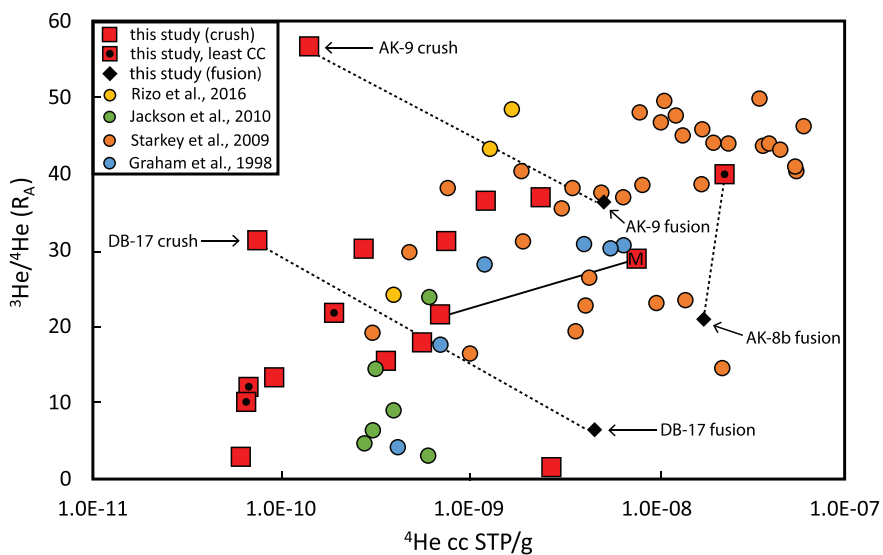


Figure 11. Helium isotopic compositions compared to ${}^4\text{He}$ concentrations for Baffin Island and West Greenland magmatic olivines. Samples with lower helium concentrations tend to have lower ${}^3\text{He}/{}^4\text{He}$, possibly due to greater sensitivity to posteruptive radiogenic ingrowth of ${}^4\text{He}$. The dashed lines connect the olivine crush experiment data to the respective fusion results for three different samples. The solid line connects a crush experiment on a single olivine megacryst (denoted by an “M” in the symbol) to the crush experiment for multiple smaller olivine phenocrysts from the same lavas (AK-13). In the key, CC signifies crustal contamination.

calculated present-day mantle ratio, of the least contaminated high- ${}^3\text{He}/{}^4\text{He}$ Baffin Island lava, sample AK-8b. Finally, paired ${}^3\text{He}/{}^4\text{He}$ and ${}^{206}\text{Pb}/{}^{204}\text{Pb}$ compositions of Baffin Island lavas with mantle-like Nb/Th and Ce/Pb do not overlap with Iceland lavas. The highest ${}^3\text{He}/{}^4\text{He}$ Baffin Island lava has Pb isotopic compositions (e.g., measured ${}^{206}\text{Pb}/{}^{204}\text{Pb} = 17.7560$) that are less radiogenic than those of the highest ${}^3\text{He}/{}^4\text{He}$ Iceland lava (e.g., ${}^{206}\text{Pb}/{}^{204}\text{Pb} = 18.653$), an observation that holds for both the measured ${}^{206}\text{Pb}/{}^{204}\text{Pb}$ and the calculated present-day ${}^{206}\text{Pb}/{}^{204}\text{Pb}$ for the Baffin Island mantle source. There is no evidence that the least contaminated Baffin Island lavas and Iceland high- ${}^3\text{He}/{}^4\text{He}$ lavas converge at a common Sr, Nd, and Pb isotopic composition, even if existing data trends are extrapolated to higher ${}^3\text{He}/{}^4\text{He}$. Unfortunately, there are insufficient existing samples with paired ${}^3\text{He}/{}^4\text{He}$ and ${}^{176}\text{Hf}/{}^{177}\text{Hf}$ to make this comparison.

4. Discussion

4.1. Two Geochemically Distinct High- ${}^3\text{He}/{}^4\text{He}$ Components in the Iceland Plume or Crustal Assimilation in Baffin Island High- ${}^3\text{He}/{}^4\text{He}$ Lavas

The highest ${}^3\text{He}/{}^4\text{He}$ lavas from Iceland (up to $47.5 R_A$; Harðardóttir et al., 2018; or $37.7 R_A$ when only considering lavas that have been characterized with paired radiogenic isotope analyses; Hilton et al., 1999), Hawaii ($35.3 R_A$; Kurz et al., 1983, 1982; Valbracht et al., 1997), Samoa ($33.8 R_A$; Farley et al., 1992; Jackson, Hart, et al., 2007; Workman et al., 2004), and Galápagos ($30.3 R_A$; Graham et al., 1993; Jackson, 2008; Kurz et al., 2014; Kurz & Geist, 1999) have distinct radiogenic isotopic compositions (see Figures 8, 9, and 12). Here we show that the radiogenic isotopic compositions of the least crustally contaminated high- ${}^3\text{He}/{}^4\text{He}$ lavas from 60 Ma Baffin Island document a mantle domain that is geochemically distinct from mid-Miocene Iceland lavas with the highest ${}^3\text{He}/{}^4\text{He}$. Thus, we argue for the presence of *two* geochemically distinct high- ${}^3\text{He}/{}^4\text{He}$ components within a single mantle plume. However, it is essential to explore whether the difference in radiogenic isotopic compositions between the least crustally contaminated Baffin Island lavas and Iceland high- ${}^3\text{He}/{}^4\text{He}$ lavas reflects temporal evolution of the high- ${}^3\text{He}/{}^4\text{He}$ mantle source sampled by the Iceland hotspot or continental crust assimilation by the Baffin Island lavas.

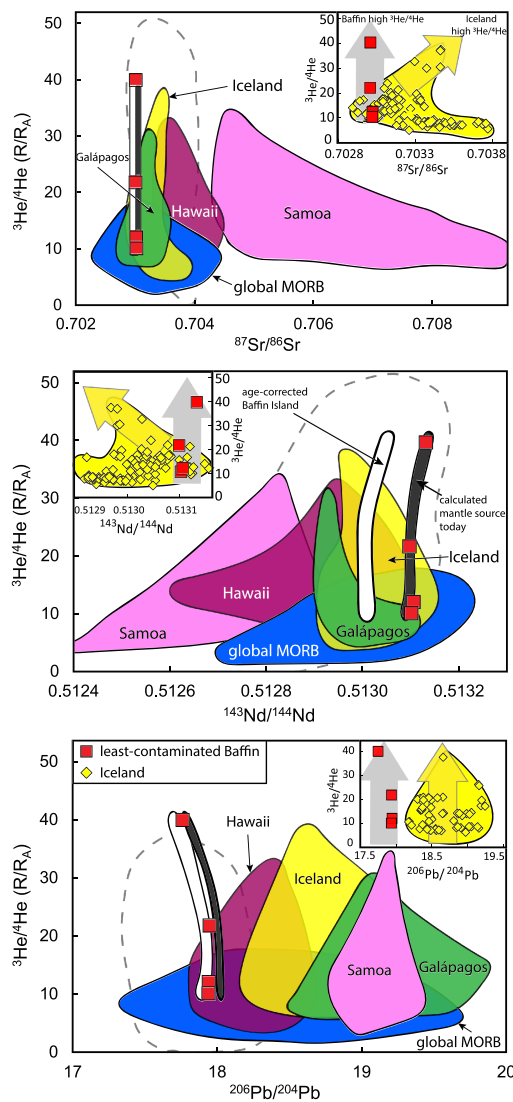


Figure 12. Helium isotopic compositions for several hotspots shown as a function of whole rock ${}^{87}\text{Sr}/{}^{86}\text{Sr}$, ${}^{143}\text{Nd}/{}^{144}\text{Nd}$, and ${}^{206}\text{Pb}/{}^{204}\text{Pb}$. Data points shown are the measured isotopic compositions, and white and dark gray fields reflect age-corrected and calculated present-day mantle source compositions, respectively; ${}^3\text{He}/{}^4\text{He}$ data are not age corrected. Lavas with the highest ${}^3\text{He}/{}^4\text{He}$ in Iceland (yellow field and symbols; note that the yellow field includes all lavas from mainland Iceland including mid-Miocene and Neovolcanic zone lavas) and the least crustally contaminated Baffin Island lavas (red squares) exhibit different Sr, Nd, and Pb isotopic compositions (the comparisons rely on measured isotopic data [red squares] and calculated present-day isotopic compositions of the mantle source of the Baffin Island lavas; see section S2.3 in the supporting information). The least crustally contaminated lavas from Baffin Island have lower ${}^{87}\text{Sr}/{}^{86}\text{Sr}$ and ${}^{206}\text{Pb}/{}^{204}\text{Pb}$, and higher ${}^{143}\text{Nd}/{}^{144}\text{Nd}$, than the highest ${}^3\text{He}/{}^4\text{He}$ Iceland lavas, suggesting a different high- ${}^3\text{He}/{}^4\text{He}$ source (see insets). The gray dashed line contains the field for Baffin Island and West Greenland lavas that are crustally contaminated ($\text{Nb}/\text{Th} < 13$, $\text{Ce}/\text{Pb} < 20$, and/or $\text{MgO} < 10 \text{ wt.\%}$), or are insufficiently characterized to identify potential crustal contamination (e.g., many Baffin Island lavas with ${}^3\text{He}/{}^4\text{He}$ data lack Pb concentration [and Pb isotopic] data; Stuart et al., 2003; Starkey et al., 2009). A global data set for oceanic lavas, including MORB and samples from the four hotspots with ${}^3\text{He}/{}^4\text{He} > 30 R_A$, are provided for context (fields are adapted from Jackson, Hart, et al., 2007; Jackson et al., 2008).

Crustal contamination is recorded in high- ${}^3\text{He}/{}^4\text{He}$ continental flood basalts associated with the Icelandic plume at Baffin Island, West Greenland, and East Greenland (e.g., Day, 2016; Larsen & Pedersen, 2009; Lightfoot et al., 1997; Peate, 2003; Yaxley et al., 2004). If the Iceland hotspot has a single high- ${}^3\text{He}/{}^4\text{He}$ component, one hypothesis is that the high- ${}^3\text{He}/{}^4\text{He}$ mantle component sampled at the Iceland hotspot has a single Sr-Nd-Hf-Pb isotopic composition over time and that the difference in Sr-Nd-Hf-Pb between Iceland and the least contaminated Baffin Island high- ${}^3\text{He}/{}^4\text{He}$ lavas is due to melts of the latter having assimilated some amount of continental crust. Radiogenic isotopic compositions for basement samples from West Greenland reported by Larsen and Pedersen (2009)—which are inferred to be similar to the basement underlying the Baffin Island picrites (St-Onge et al., 2009)—allow a test of this hypothesis by investigating the influence of crustal contamination on the radiogenic isotopic compositions of Baffin Island lavas.

The four least contaminated Baffin Island lavas have lower ${}^{87}\text{Sr}/{}^{86}\text{Sr}$ (0.703009) than the highest ${}^3\text{He}/{}^4\text{He}$ ($37 R_A$) Iceland lava with available ${}^{87}\text{Sr}/{}^{86}\text{Sr}$ data (0.703465 for sample SEL97; Hilton et al., 1999). The shift to lower ${}^{87}\text{Sr}/{}^{86}\text{Sr}$ in the least contaminated, highest ${}^3\text{He}/{}^4\text{He}$ Baffin Island lava cannot be explained by continental crust assimilation because assimilation of the local Precambrian crust (which has very high ${}^{87}\text{Sr}/{}^{86}\text{Sr}$ —0.713758 to 0.823010—compared to the least crustally contaminated Baffin Island lavas, 0.703008 to 0.703021) would only serve to *increase* the Baffin Island ${}^{87}\text{Sr}/{}^{86}\text{Sr}$, not decrease it (Figure 8). Therefore, lower ${}^{87}\text{Sr}/{}^{86}\text{Sr}$ in the least crustally contaminated high- ${}^3\text{He}/{}^4\text{He}$ Baffin Island lavas relative to high- ${}^3\text{He}/{}^4\text{He}$ Iceland lavas must relate to differences in their respective mantle source compositions, an observation that holds for both measured and age-corrected ${}^{87}\text{Sr}/{}^{86}\text{Sr}$ in Baffin Island lavas, as well as calculated present-day ${}^{87}\text{Sr}/{}^{86}\text{Sr}$ of the Baffin Island mantle source (Figure 12). This argument does not exclude a small contribution of continental crust assimilation in the four least crustally contaminated Baffin Island lavas. Rather, invoking this would only enforce the argument that Baffin Island and Iceland high- ${}^3\text{He}/{}^4\text{He}$ lavas have distinct ${}^{87}\text{Sr}/{}^{86}\text{Sr}$, because any crustal contamination in Baffin Island lavas would be expected to increase the ${}^{87}\text{Sr}/{}^{86}\text{Sr}$, suggesting that hypothetical uncontaminated versions of these lavas would have *even lower* ${}^{87}\text{Sr}/{}^{86}\text{Sr}$ relative to the high- ${}^3\text{He}/{}^4\text{He}$ Iceland lavas.

Neodymium isotopic compositions of Baffin Island lavas lead to a similar conclusion. The measured (and calculated Baffin mantle source today) ${}^{143}\text{Nd}/{}^{144}\text{Nd}$ of the four least crustally contaminated high- ${}^3\text{He}/{}^4\text{He}$ lavas from Baffin Island have higher ${}^{143}\text{Nd}/{}^{144}\text{Nd}$ than high- ${}^3\text{He}/{}^4\text{He}$ Iceland lavas (Figure 12), an observation that also cannot be explained by crustal assimilation because continental crust—which has very low ${}^{143}\text{Nd}/{}^{144}\text{Nd}$ (0.510737 to 0.511945) compared to the least crustally contaminated Baffin Island lavas (0.513094 to 0.513128)—would lower the ${}^{143}\text{Nd}/{}^{144}\text{Nd}$ of the Baffin Island lavas (Figure 8). Thus, the observation of a more geochemically depleted high- ${}^3\text{He}/{}^4\text{He}$ component in the proto-Iceland plume, compared to the mid-Miocene to modern Iceland plume, is consistent for both ${}^{143}\text{Nd}/{}^{144}\text{Nd}$ and ${}^{87}\text{Sr}/{}^{86}\text{Sr}$. Unfortunately, too few Hf isotopic data exist to verify that this also holds true for ${}^{176}\text{Hf}/{}^{177}\text{Hf}$.

In ${}^3\text{He}/{}^4\text{He}$ versus ${}^{206}\text{Pb}/{}^{204}\text{Pb}$ isotopic space, there is no overlap in the ${}^{206}\text{Pb}/{}^{204}\text{Pb}$ compositions of the least contaminated Baffin Island lavas

and the Iceland field (Figure 12). It is equally important to evaluate whether the difference in Pb isotopic compositions between Iceland and Baffin Island lavas relates to continental crust assimilation, because Pb isotopes in basalts can be more susceptible to the compositional effects of crustal assimilation than Sr and Nd isotopes. Indeed, Pb is ~60 times more concentrated in the average West Greenland basement (from Larsen & Pedersen, 2009) than in the least contaminated Baffin Island lavas, whereas Sr and Nd are only ~3 and ~5 times, respectively, more concentrated in the former compared to the latter. Therefore, it is crucial to test the hypothesis that Iceland and Baffin Island high-³He/⁴He mantle sources actually have the same Pb isotopic compositions and that the apparent shift to lower ²⁰⁶Pb/²⁰⁴Pb in Baffin Island lavas is due to assimilation of continental crust with less radiogenic Pb. To test this hypothesis, a mixing model combines basement material from Larsen and Pedersen (2009) with the composition of the highest ³He/⁴He lava (with measured Sr-Nd-Pb isotopes) from Iceland (Hilton et al., 1999; see section S3.1 and Figure S4 in the supporting information). While crustal assimilation of an Iceland high-³He/⁴He lava composition can generate the Pb isotopic compositions of the least contaminated Baffin Island lavas (Figure S4), it also generates strong crustal contamination signatures (i.e., low continental-like ratios) in Ce/Pb and Nb/Th that are not seen in the least crustally contaminated Baffin lavas (section S3.1.). In this light, we find that there is no basement composition in this data set that, through crustal assimilation, can explain the Sr-Nd-Pb isotopic shift from the composition of the highest ³He/⁴He Iceland lava to the least contaminated Baffin Island lavas while also generating the mantle-like Ce/Pb and Nb/Th observed in the same lavas (Figure S4). Furthermore, the observation of mantle-like Ce/Pb, Nb/Th, and δ¹⁸O in the four least contaminated Baffin Island lavas suggests that these four Baffin Island lavas have assimilated very little, if any, continental crust. We conclude that the four Baffin Island lavas are likely very close in composition to their original uncontaminated compositions and that, hence, the Pb isotopic composition of their mantle source must be less radiogenic than (and therefore isotopically distinct from) Iceland high-³He/⁴He lavas.

It is important to acknowledge that our application of strict trace elements filters, applied to avoid Baffin Island lavas that may have experienced crustal assimilation, may have also filtered out lavas with primary “enriched mantle” (EM) signatures, which have been suggested to exist in the Baffin Island mantle (Kent et al., 2004; Robillard et al., 1992; Starkey et al., 2009, 2012). For example, the enriched mantle (with higher ⁸⁷Sr/⁸⁶Sr and lower ¹⁴³Nd/¹⁴⁴Nd) has low Ce/Pb and Nb/Th due to continental crust recycling (Hofmann, 1997; Jackson, Hart, et al., 2007) and any uncontaminated Baffin Island primary melts sampling EM domains with low mantle-derived Ce/Pb and Nb/Th could potentially be eliminated from consideration due to the strict crustal assimilation filters applied to the data set. However, even if enriched mantle lavas with low Ce/Pb and Nb/Th have been filtered out from the Baffin Island data set, this does not negate the finding of a high-³He/⁴He component in Baffin Island that is *more geochemically depleted* than the Iceland high-³He/⁴He component (Figure 12): the observation remains that there are high-³He/⁴He Baffin Island lavas with lower ⁸⁷Sr/⁸⁶Sr and higher ¹⁴³Nd/¹⁴⁴Nd that are more geochemically depleted than high-³He/⁴He Iceland lavas, and these isotopic differences cannot be explained by crustal assimilation. This supports prior suggestions of a depleted component in the Baffin Island flood basalt suite (Starkey et al., 2009; Kent et al., 2004).

4.2. A Heterogeneous High-³He/⁴He Component: Implications for a Common Component in the Mantle and the Origins of Its Geochemically Depleted Nature

It is intriguing that, among the highest ³He/⁴He hotspot localities with ³He/⁴He > 30 R_A (Hawaii, Galápagos, Samoa, and Iceland), the least crustally contaminated Baffin Island lavas have the lowest ²⁰⁶Pb/²⁰⁴Pb and the most geochemically depleted ⁸⁷Sr/⁸⁶Sr and ¹⁴³Nd/¹⁴⁴Nd (see Figures 8, 9, and 12). These observations provide important clues to the origin of the high-³He/⁴He mantle domain. For example, it could be that the extent of geochemical depletion relates to the process that generated high-³He/(U + Th)—and thus enabling preservation of high ³He/⁴He—in the Baffin Island mantle source. If He is less incompatible than U and Th during mantle melting (e.g., Parman et al., 2005), then greater geochemical depletion will result in higher ³He/⁴He and higher ¹⁴³Nd/¹⁴⁴Nd, consistent with the highest ³He/⁴He preserved in Baffin Island lavas with higher ¹⁴³Nd/¹⁴⁴Nd than observed at other high-³He/⁴He hotspots. However, other studies examining the partitioning of helium during mantle melting suggest that He is more incompatible than U and Th (Heber et al., 2007; Jackson et al., 2013). Thus, an alternative model for the highly geochemically depleted Sr and Nd (and unradiogenic Pb) isotopes in Baffin Island lavas, compared to other high-³He/⁴He OIB, is that

variable quantities of enriched lithospheric material (e.g., recycled oceanic and/or continental crust) were added to an initially homogeneous, geochemically depleted high- $^3\text{He}/^4\text{He}$ mantle source (like that seen in Baffin Island lavas) to produce the Sr-Nd-Hf-Pb isotopic variability observed in high- $^3\text{He}/^4\text{He}$ ($>30 R_A$) lavas at Hawaii, Galápagos, Samoa, and Iceland (Garapić et al., 2015). A similar conclusion was drawn by Trela et al. (2015) to explain secular cooling of the Galápagos plume as addition of recycled material would decrease the buoyancy (and therefore ascent rate) of rising plume material. Consistent with this alternative scenario, radiogenic $^{206}\text{Pb}/^{204}\text{Pb}$ in the high- $^3\text{He}/^4\text{He}$ Iceland component, compared to Baffin Island lavas, could result from the addition of a high-U/Pb component. Recycled oceanic crust is an obvious candidate for the high-U/Pb material and would help explain the elevated Ti in high- $^3\text{He}/^4\text{He}$ OIB lavas relative to Baffin Island (Garapić et al., 2015) and the recycled atmospheric heavy noble gas signatures in a moderately high- $^3\text{He}/^4\text{He}$ Icelandic lava (Mukhopadhyay, 2012) and in high- $^3\text{He}/^4\text{He}$ Samoan plume-related lavas in the Lau Basin (Pető et al., 2013). This is further supported by combined trace element modeling and geophysical observations that show a recycled component in mainland Iceland lavas (Shortle et al., 2014). In this scenario, Baffin Island lavas sample the most pristine (or “least modified”; White, 2015) surviving relic of an early formed, geochemically depleted high- $^3\text{He}/^4\text{He}$ mantle domain that has experienced the least overprinting by recycled material over geologic time. Recent measurements of δD in high- $^3\text{He}/^4\text{He}$ lavas show that some high- $^3\text{He}/^4\text{He}$ lavas retain primordial δD , while others sample a recycled water component, illustrating that high- $^3\text{He}/^4\text{He}$ lavas are known to contain signatures of varying amounts of recycled material (Loewen et al., 2019). Heavy noble gases would provide an ideal test of this hypothesis. $^{129}\text{Xe}/^{130}\text{Xe}$ data are available for a moderately high- $^3\text{He}/^4\text{He}$ ($17.2 R_A$) lava from the neovolcanic zone of Iceland and a Lau Basin high- $^3\text{He}/^4\text{He}$ lava ($28.1 R_A$; Pető et al., 2013), and they indicate both an early Hadean component in the respective mantle sources and the presence of recycled atmospheric heavy noble gases. Unfortunately, the heavy noble gas compositions of Baffin Island lavas have not yet been analyzed, rendering premature the use of heavy noble gases to evaluate whether the Baffin Island high- $^3\text{He}/^4\text{He}$ mantle domain has experienced less overprinting by recycled materials compared to other high- $^3\text{He}/^4\text{He}$ hotspot lavas. Conclusions regarding a recycled atmospheric heavy noble gas component in the highest $^3\text{He}/^4\text{He}$ mantle domain (e.g., Mukhopadhyay & Parai, 2019) might benefit from measurements targeting the Baffin Island-West Greenland suite.

The addition of recycled material to depleted mantle, as inferred for the high- $^3\text{He}/^4\text{He}$ Baffin Island lavas, has implications for the origin of Sr-Nd-Pb isotopic heterogeneity in high- $^3\text{He}/^4\text{He}$ lavas and the “common component” sampled by hotspots. In Sr-Nd-Pb isotopic space, different hotspots form “arrays” that converge on a common region, referred to as FOZO (focus zone; Hart et al., 1992) or C (common; Hanan & Graham, 1996), and hotspot lavas that sample this common composition are suggested to host high $^3\text{He}/^4\text{He}$ (Hart et al., 1992). However, the new data from Baffin Island, combined with previously published data from the Iceland hotspot, do not seem to be consistent with convergence on a common high- $^3\text{He}/^4\text{He}$ component in Sr-Nd-Pb isotopic space: arrays formed by Iceland and Baffin Island high- $^3\text{He}/^4\text{He}$ lavas diverge with increasing $^3\text{He}/^4\text{He}$ in Figure 12. Rather than a homogeneous high- $^3\text{He}/^4\text{He}$ domain sampled by all hotspots, a model of heterogeneity in the high- $^3\text{He}/^4\text{He}$ domain, that incorporates the addition of heterogeneous recycled materials to a mantle component similar to Baffin Island, may be more consistent with the observed intrahotspot heterogeneity in the high- $^3\text{He}/^4\text{He}$ domain(s) sampled by Iceland, and the interhotspot Sr-Nd-Pb heterogeneity observed in the highest $^3\text{He}/^4\text{He}$ lavas from hotspots globally (Jackson, Kurz, et al., 2007; Figure 12).

The origin of the geochemically depleted radiogenic isotopic signatures of lavas with primitive $^3\text{He}/^4\text{He}$ has eluded explanation since the first geochemical characterization of high- $^3\text{He}/^4\text{He}$ lavas (Kurz et al., 1982). With the exception of $^3\text{He}/^4\text{He}$ and ^{182}W (but for ^{182}W see section 4.3), the least crustally contaminated Baffin Island picrites resemble MORB in all radiogenic isotopic spaces explored here (Figures 8 and 9; Ellam & Stuart, 2004), as well as $^{142}\text{Nd}/^{144}\text{Nd}$ (de Leeuw et al., 2017), $^{187}\text{Os}/^{188}\text{Os}$ (Dale et al., 2009), and stable isotopes (e.g., $\delta^{18}\text{O}$, this study, and $\delta^{56}\text{Fe}$ and $\delta^{66}\text{Zn}$, McCoy-West et al., 2018). One hypothesis is that the proto-Iceland plume head incorporated significant upper mantle material, which would have been enhanced by concurrent rifting (e.g., Keen et al., 2012), with the result that the upper mantle dominates the non-noble gas isotopic signatures in erupted lavas; the high- $^3\text{He}/^4\text{He}$ signature from the deep mantle source was retained due to higher concentrations of helium in the deep mantle relative to the upper

mantle (Stuart et al., 2003, 2000; section S3.2 of the supporting information). In this model, the composition of the deep mantle domain contributing high $^3\text{He}/^4\text{He}$ to the depleted mantle is unknown because it has been almost completely overprinted—for everything except for noble gases and possibly W—by mixing with the depleted upper mantle.

Alternatively, an intrinsic depleted component (distinct from the upper mantle MORB source) may reside in the Iceland plume (e.g., Fitton et al., 2003), and if this component hosts elevated $^3\text{He}/^4\text{He}$, it provides an alternative explanation for the geochemically depleted nature of high- $^3\text{He}/^4\text{He}$ material in the Iceland plume. PREMA (Prevalent Mantle) was suggested to be a geochemically depleted lower mantle component sampled by mantle plumes that overlaps with the radiogenic composition of Icelandic high- $^3\text{He}/^4\text{He}$ lavas (Zindler & Hart, 1986). One model proposed for the origin of PREMA is that it is the depleted residue of “significant differentiation of the silicate portion of the Earth [that] occurred contemporaneously with core segregation ... and might represent the most primitive remaining mantle, having essentially survived unscathed since the earliest days of Earth history” (Zindler & Hart, 1986). In this model, PREMA in the upper mantle convective regime continued to be depleted by crustal extraction and evolved toward depleted MORB mantle (DMM; Zindler & Hart, 1986). If the least contaminated Baffin Island lavas sample PREMA that was preserved in the lower mantle, the short-lived $^{142}\text{Nd}/^{144}\text{Nd}$ system (where ^{146}Sm decays to ^{142}Nd , $t_{1/2} = 103$ Ma), sensitive to Hadean silicate differentiation, permits investigation of early differentiation that might have generated the geochemically depleted mantle domain with high $^3\text{He}/^4\text{He}$. However, no resolvable $^{142}\text{Nd}/^{144}\text{Nd}$ anomalies are observed in either Baffin Island (de Leeuw et al., 2017) or Iceland (Andreasen et al., 2008; Debaille et al., 2007). The implications of the lack of observable $^{142}\text{Nd}/^{144}\text{Nd}$ anomalies in Iceland hotspot lavas (which contrasts with resolvable $^{142}\text{Nd}/^{144}\text{Nd}$ variability at other hotspots; Horan et al., 2018; Peters et al., 2018) are not yet clear, but may still leave open the possibility of Baffin Island lavas sampling the depleted residue of Hadean terrestrial differentiation (see section S3.2.), which in turn would be consistent with the primitive Pb isotopic compositions of the least crustally contaminated Baffin Island lavas (Jackson et al., 2010; this study).

4.3. Location of the High- $^3\text{He}/^4\text{He}$ Mantle Domains Sampled by the Iceland Plume

While it is important to define heterogeneity that exists within the highest $^3\text{He}/^4\text{He}$ domain in the mantle, it is also important to constrain *where* the heterogeneous high- $^3\text{He}/^4\text{He}$ domains reside within the mantle. Relationships between $^3\text{He}/^4\text{He}$ and geophysical observations at hotspots can provide a clue regarding the location of these domains in the mantle. The hotspot localities with greater contributions from the FOZO-C components (inferred to have high $^3\text{He}/^4\text{He}$) have lower seismic shear wave velocity anomalies in the shallow (200 km) upper mantle (Konter & Becker, 2012) and higher buoyancy flux than lower $^3\text{He}/^4\text{He}$ hotspots (Graham, 2002; Jackson et al., 2017; Jellinek & Manga, 2004; Putirka et al., 2007), which is consistent with higher $^3\text{He}/^4\text{He}$ hotspots sampling hotter mantle domains than lower $^3\text{He}/^4\text{He}$ hotspots and MORB (Putirka, 2008; Jackson et al., 2017). Here we examine whether the highest $^3\text{He}/^4\text{He}$ hotspot lavas sampled at Baffin Island-West Greenland also sample a mantle source that was hotter than ambient mantle sampled by MORB (Herzberg & Gazel, 2009; Holm et al., 1993; Putirka et al., 2007; Trela et al., 2017). Using the approach of Herzberg and Asimow (2015), we explore the hypothesis of a hotter-than-ambient-mantle high- $^3\text{He}/^4\text{He}$ plume by comparing calculated mantle potential temperatures from (1) the least crustally contaminated Baffin Island-West Greenland compositions and (2) highly magnesian MORB from the Siqueiros transform fault that show a clear olivine liquid line of descent. The calculated mantle potential temperatures for the least contaminated Baffin Island-West Greenland primary melts range from 1510 to 1630 °C. This range of temperatures is consistent with previously calculated mantle potential temperatures for proto-Iceland plume lavas from Larsen and Pedersen (2000; 1520 to 1560 °C), Herzberg and Gazel (2009; 1470 to 1650 °C), Hole and Millett (2016; 1480 to 1550 °C), and Putirka et al. (2018; 1630 ± 65 °C). Critically, the Baffin Island-West Greenland lavas yield higher calculated mantle potential temperatures than the high-MgO Siqueiros MORB considered here (1300 to 1410 °C), the Siqueiros MORB data set examined by Putirka et al. (2018; 1420 ± 40 °C), the compiled MORB in Madrigal et al. (2016; 1320 to 1390 °C), and average MORB from Cottrell and Kelley (2011; 1320 ± 39 °C).

Hotter mantle potential temperatures result in higher degrees of melting at Baffin Island and West Greenland (10–30%, based on results from the PRIMELT3 calculations for the Baffin Island and West Greenland in Figure 3) relative to high-MgO Siqueiros MORB (5–20%, using PRIMELT3 and lavas in

Figure 3). Higher degrees of melting in Baffin Island lavas relative to MORB explain lower primary liquid Na₂O compositions in the former compared to the latter (e.g., Klein & Langmuir, 1987; see Figure 3). Similarly, higher mantle potential temperatures will result in greater average melting depths for the Baffin Island-West Greenland lavas compared to MORB, consistent with higher calculated primary melt FeO in the former (i.e., Klein & Langmuir, 1987; see Figure 3). Compared to calculated primary MORB melts, higher temperature of melting in the Baffin Island-West Greenland lavas can also explain higher MgO (owing to higher degrees of melting driving melt closer to olivine compositions), lower SiO₂ (owing to reduced silica activity at greater melting depths), lower Al₂O₃ (due to greater extent of melting in the garnet stability field, thereby leaving Al₂O₃ retained in the source), and lower CaO (because the clinopyroxene-phase volume increases at higher-pressure melting at the expense of olivine and orthopyroxene; for example, Walter, 1998) (see Figure 3). These findings help to explain the rather large differences in the primary liquid major element compositions between MORB (located far from hotspots) and the least crustally contaminated Baffin Island-West Greenland lavas (Figures 2 and 3), and are consistent with the hypothesis that the high-³He/⁴He domain is sampled by hot plumes (Jackson et al., 2017; Putirka, 2008).

A remaining question is why high-³He/⁴He hotspots are hotter than both low-³He/⁴He hotspots (Jackson et al., 2017) and MORB located far from hotspots. One hypothesis is that primitive domains are preserved in deep, dense mantle reservoirs (Deschamps et al., 2011; Jellinek & Manga, 2004; Samuel & Farnetani, 2003), and only the hottest mantle plumes are sufficiently buoyant to entrain this material from the deep mantle (Jackson et al., 2017). A deep dense domain is ideally suited for preserving primitive geochemical signatures that, like ³He/⁴He, record the earliest history of the planet despite billions of years of mantle convective mixing. For example, the highest ³He/⁴He lavas from Iceland, Samoa, and Hawaii exhibit negative ¹⁸²W anomalies relative to the terrestrial standard (Mundl et al., 2017), and these ¹⁸²W anomalies date to within ~60 Ma of terrestrial accretion. In order for modern OIB to have high ³He/⁴He and ¹⁸²W anomalies, there must be domains capable of preserving ancient geochemical signatures within the Earth; however, the exact locations of these domains remain unknown.

Two large low-shear-velocity provinces (LLSVPs) that are consistently observed in seismic tomography studies of the deepest mantle (Garnero & McNamara, 2008; Lekic et al., 2012; McNamara, 2019) may represent storage sites for less degassed and ancient mantle material, as well as younger subducted oceanic or continental crust (e.g., Li et al., 2014). Garapić et al. (2015) observed that the highest ³He/⁴He hotspots lie above or near the margins of the LLSVPs and used this observation to suggest that these hotspots sample elevated ³He/⁴He from the LLSVPs. Based on a geographic relationship between hotspots with elevated ³He/⁴He and the location of LLSVPs, LLSVPs have been argued to host elevated ³He/⁴He (Williams et al., 2019). If LLSVPs contain primitive geochemical signatures (Tackley, 2000), as well as pockets of heterogenous recycled materials, then variable mixing of primitive and recycled components within LLSVPs could explain the Sr-Nd-Pb-Hf isotopic differences observed between the least contaminated high-³He/⁴He lavas from Baffin Island-West Greenland and the highest ³He/⁴He OIB lavas at Iceland, Hawaii, Samoa, and Galápagos (Garapić et al., 2015). More importantly for this study, the juxtaposition (and possible mixing) of ancient high-³He/⁴He and recycled domains in the plume source could explain the isotopic heterogeneity in the Iceland plume through time. Moreover, ultralow velocity zones (ULVZ; Garnero et al., 2016; McNamara et al., 2010; Rost et al., 2005), which have even slower shear wave velocity anomalies than LLSVPs, provide a second potential long-term storage site for primitive geochemical signatures (Herzberg et al., 2013; Mundl et al., 2017); the three hotspots observed to have ¹⁸²W anomalies—Hawaii, Iceland, and Samoa—are all associated with ULVZs (Mundl et al., 2017; Mundl-Petermeier et al., 2019). (Note that ¹⁸²W data are not yet available for Galápagos lavas.) Alternatively, highly viscous mantle domains could lead to the production of isolated convection cells in the mantle, ranging from ~1,000 to 2,200 km depth, called bridgmanite-enriched ancient mantle structures, or BEAMS (Ballmer et al., 2017). Long-term stability of highly viscous portions of the mantle, like BEAMS, may also serve as a storage site for geochemical domains over billions of years. However, further work is needed to explore why material from BEAMS would be preferentially sampled by only the hottest, most buoyant mantle plumes. A contribution from one or more of these domains to rising plume conduits may explain how some isotopic signatures, such as high ³He/⁴He and ¹⁸²W, have escaped homogenization and have been observed in mantle-derived rocks that erupted during the Cenozoic.

The core is an additional possible residence site for both elevated ${}^3\text{He}/{}^4\text{He}$ and negative ${}^{182}\text{W}$ anomalies. The possibility of the core as a source of primitive helium in mantle plumes has been amply explored (e.g., Bouhifd et al., 2013; Hofmann et al., 1986; Jephcoat, 1998; Porcelli & Halliday, 2001; Roth et al., 2019). Tungsten is moderately siderophile and therefore partitioned into the core during core formation, resulting in a low Hf/W ratio (and thus negative ${}^{182}\text{W}$ anomalies) in the core relative to the bulk silicate Earth. Hence, a core contribution to mantle plumes would be observed as negative ${}^{182}\text{W}$ anomalies in hotspot lavas. Mundl et al. (2017) and Mundl-Petermeier et al. (2019) reported negative ${}^{182}\text{W}$ anomalies in high- ${}^3\text{He}/{}^4\text{He}$ Iceland lavas, consistent with a core contribution, whereas Rizo et al. (2016) reported positive ${}^{182}\text{W}$ anomalies in Baffin Island lavas. However, Kruijer and Kleine (2018) proposed a potential nuclear field shift effect as the origin of the large $\mu^{182}\text{W}$ found in an Ontong Java Plateau drill core sample (Rizo et al., 2016), leading to these authors speculating about the validity of the large positive $\mu^{182}\text{W}$ anomaly measured in the Baffin Island sample from the same study. The Rizo et al. (2016) result contrasts with recent results of Mundl-Petermeier et al. (2019), which show slightly negative ${}^{182}\text{W}$ anomalies in genetically related West Greenland picrites. Given the susceptibility of ${}^{182}\text{W}$ in primitive Baffin Island and West Greenland lavas (≤ 62 ppb W; Mundl-Petermeier et al., 2019; Rizo et al., 2016) to being overprinted by continental crust (1,000 ppb W; Rudnick & Gao, 2003), additional ${}^{182}\text{W}$ analyses from Baffin Island lavas, specifically targeting lavas that are identified as being least crustally contaminated, will be critical for evaluating the presence of $\mu^{182}\text{W}$ anomalies in the mantle source of Baffin Island lavas.

If additional targeting of the least crustally contaminated Baffin Island lavas reveals anomalous ${}^{182}\text{W}$ consistent with a core contribution, further investigation of the physical processes and potential geochemical indicators of a core contribution to the mantle will be needed to further assess this hypothesis. For example, it will also require explanation of the lack of extreme highly siderophile element (HSE: Ru, Rh, Pd, Re, Os, Ir, Pt, and Au) enrichment in high- ${}^3\text{He}/{}^4\text{He}$ lavas expected from a core contribution (e.g., Rizo et al., 2019). It will further be important to understand the mechanism that links anomalous ${}^{182}\text{W}$, high ${}^3\text{He}/{}^4\text{He}$, and the hottest/most buoyant plumes (i.e., if the high- ${}^3\text{He}/{}^4\text{He}$ mantle domain is denser and has anomalous ${}^{182}\text{W}$, what is the mechanism responsible for the elevated density and how did it acquire anomalous ${}^{182}\text{W}$?).

5. Conclusions

The Iceland hotspot has erupted high- ${}^3\text{He}/{}^4\text{He}$ for over 60 Myr, providing a natural laboratory for investigation of time-integrated chemical evolution in a high- ${}^3\text{He}/{}^4\text{He}$ mantle plume. After filtering out Baffin Island-West Greenland lavas that are influenced by continental crust contamination, the least crustally contaminated Baffin Island-West Greenland lavas host a geochemically depleted high- ${}^3\text{He}/{}^4\text{He}$ component that is more depleted than any other high- ${}^3\text{He}/{}^4\text{He}$ lavas globally, including high- ${}^3\text{He}/{}^4\text{He}$ lavas from Iceland. Compositional differences between the least crustally contaminated, high- ${}^3\text{He}/{}^4\text{He}$ Baffin Island-West Greenland lavas and high- ${}^3\text{He}/{}^4\text{He}$ mainland Iceland lavas cannot be explained by crustal contamination of the former, indicating temporal evolution of the radiogenic isotopic composition of the high- ${}^3\text{He}/{}^4\text{He}$ component in the Iceland hotspot. Furthermore, there is no evidence for compositional convergence of Baffin Island-West Greenland high- ${}^3\text{He}/{}^4\text{He}$ lavas and Iceland high- ${}^3\text{He}/{}^4\text{He}$ lavas. Therefore, high- ${}^3\text{He}/{}^4\text{He}$ lavas from the Iceland hotspot do not support a homogeneous high- ${}^3\text{He}/{}^4\text{He}$ component in the modern mantle. Geochemically distinct high- ${}^3\text{He}/{}^4\text{He}$ domains within the Iceland hotspot suggests the plume has sampled at least two high- ${}^3\text{He}/{}^4\text{He}$ domains with distinct Sr-Nd-Pb and, by extension, likely also Hf, isotopic compositions over time. The origin of the geochemically highly depleted radiogenic isotopic compositions in Baffin Island-West Greenland high- ${}^3\text{He}/{}^4\text{He}$ lavas remains an important outstanding question, but may relate to incorporation of depleted upper mantle during melting in a rift environment and preservation of elevated ${}^3\text{He}/{}^4\text{He}$ due to much higher helium concentrations in the high- ${}^3\text{He}/{}^4\text{He}$ plume compared to the upper mantle. Alternatively, the geochemically depleted nature of high- ${}^3\text{He}/{}^4\text{He}$ Baffin Island lavas, the highest on record, may reflect a depleted deep mantle domain to which subsequent variable addition of recycled materials has generated the isotopic heterogeneity observed in high- ${}^3\text{He}/{}^4\text{He}$ lavas from other hotspots. Finally, it is also found that Baffin Island and related West Greenland lavas, which host elevated ${}^3\text{He}/{}^4\text{He}$, record hotter temperatures (1510 to 1630 °C) than Siqueiros MORB (1320 to 1480 °C), consistent with a deep, dense origin for the high- ${}^3\text{He}/{}^4\text{He}$ mantle domain sampled by the Iceland plume.

Acknowledgments

We acknowledge support from NSF EAR-1624840 (to M.G.J.), NSF EAR-1900652 (to M.G.J.), and NSF OCE-1259218 (to M.D.K.). We thank Don Francis for generously providing us access to his collection of Baffin Island lavas. We appreciate helpful discussion and feedback from Roberta Rudnick, Matthew Rioux, Douglas Wilson, and Keith Putirka. Jonathan Pinko is thanked for his help with sample preparation. Rick Carlson's continued generosity is gratefully acknowledged, especially discussions regarding $^{142}\text{Nd}/^{144}\text{Nd}$ evolution in the Earth. We acknowledge Al Hofmann for suggesting the use of Nb/Th, instead of Nb/U, in older rocks. We are grateful for helpful discussion with Maud Boyet while in Paris celebrating one of the author's birthdays. We thank Lotte Larsen and Asger Pedersen for advice and discussion regarding West Greenland samples. We thank C. Herzberg and G. Fitton for thorough and helpful reviews, which greatly improved this manuscript. All data published in this manuscript are available in the EarthChem data repository (<https://doi.org/10.1594/IEDA/111373>).

References

- Andreasen, R., Sharma, M., Subbarao, K. V., & Viladkar, S. G. (2008). Where on Earth is the enriched Hadean reservoir? *Earth and Planetary Science Letters*, 266(1–2), 14–28. <https://doi.org/10.1016/j.epsl.2007.10.009>
- Ballmer, M. D., Houser, C., Hernlund, J. W., Wentzcovitch, R. M., & Hirose, K. (2017). Persistence of strong silica-enriched domains in the Earth's lower mantle. *Nature Geoscience*, 10(3), 236–240. <https://doi.org/10.1038/ngeo2898>
- Bas, M. J. L., Maitre, R. W. L., Streckeisen, A., & Zanettin, B. (1986). A chemical classification of volcanic rocks based on the total alkali-silica diagram. *Journal of Petrology*, 27(3), 745–750. <https://doi.org/10.1093/petrology/27.3.745>
- Bernstein, S., Hanghøj, K., Kelemen, P. B., & Brooks, C. K. (2006). Ultra-depleted, shallow cratonic mantle beneath West Greenland: Dunitic xenoliths from Ubekendt Ejland. *Contributions to Mineralogy and Petrology*, 152(3), 335–347. <https://doi.org/10.1007/s00410-006-0109-0>
- Blichert-Toft, J., Zanda, B., Ebel, D. S., & Albarède, F. (2010). The Solar System primordial lead. *Earth and Planetary Science Letters*, 300(1–2), 152–163. <https://doi.org/10.1016/j.epsl.2010.10.001>
- Bouhifd, M. A., Jephcoat, A. P., Heber, V. S., & Kelley, S. P. (2013). Helium in Earth's early core. *Nature Geoscience*, 6(11), 982–986. <https://doi.org/10.1038/ngeo1959>
- Bouvier, A., Vervoort, J. D., & Patchett, P. J. (2008). The Lu-Hf and Sm-Nd isotopic composition of CHUR: Constraints from unequilibrated chondrites and implications for the bulk composition of terrestrial planets. *Earth and Planetary Science Letters*, 273(1–2), 48–57. <https://doi.org/10.1016/j.epsl.2008.06.010>
- Class, C., & Goldstein, S. L. (2005). Evolution of helium isotopes in the Earth's mantle. *Nature*, 436(7054), 1107–1112. <https://doi.org/10.1038/nature03930>
- Cottrell, E., & Kelley, K. A. (2011). The oxidation state of Fe in MORB glasses and the oxygen fugacity of the upper mantle. *Earth and Planetary Science Letters*, 305(3), 270–282. <https://doi.org/10.1016/j.epsl.2011.03.014>
- Dale, C. W., Pearson, D. G., Starkey, N. A., Stuart, F. M., Ellam, R. M., Larsen, L. M., et al. (2009). Osmium isotopes in Baffin Island and West Greenland picrites: Implications for the $^{187}\text{Os}/^{188}\text{Os}$ composition of the convecting mantle and the nature of high $^3\text{He}/^4\text{He}$ mantle. *Earth and Planetary Science Letters*, 278(3–4), 267–277. <https://doi.org/10.1016/j.epsl.2008.12.014>
- Day, J. M. D. (2016). Evidence against an ancient non-chondritic mantle source for North Atlantic Igneous Province lavas. *Chemical Geology*, 440, 91–100. <https://doi.org/10.1016/j.chemgeo.2016.07.002>
- de Leeuw, G. A. M., Ellam, R. M., Stuart, F. M., & Carlson, R. W. (2017). $^{142}\text{Nd}/^{144}\text{Nd}$ inferences on the nature and origin of the source of high $^3\text{He}/^4\text{He}$ magmas. *Earth and Planetary Science Letters*, 472, 62–68. <https://doi.org/10.1016/j.epsl.2017.05.005>
- Debaille, V., Brandon, A. D., Yin, Q. Z., & Jacobsen, B. (2007). Coupled $^{142}\text{Nd}/^{143}\text{Nd}$ evidence for a protracted magma ocean in Mars. *Nature*, 450(7169), 525–528. <https://doi.org/10.1038/nature06317>
- Deschamps, F., Kaminski, E., & Tackley, P. J. (2011). A deep mantle origin for the primitive signature of ocean island basalt. *Nature Geoscience*, 4(12), 879–882. <https://doi.org/10.1038/ngeo1295>
- Eiler, J. M. (2001). Oxygen isotope variations of basaltic lavas and upper mantle rocks. *Reviews in Mineralogy and Geochemistry*, 43(1), 319–364. <https://doi.org/10.2138/gsrmg.43.1.319>
- Ellam, R. M., & Stuart, F. M. (2004). Coherent He-Nd-Sr isotope trends in high $^3\text{He}/^4\text{He}$ basalts: Implications for a common reservoir, mantle heterogeneity and convection. *Earth and Planetary Science Letters*, 228(3–4), 511–523. <https://doi.org/10.1016/j.epsl.2004.10.020>
- Farley, K. A., Natland, J. H., & Craig, H. (1992). Binary mixing of enriched and undegassed (primitive?) mantle components (He, Sr, Nd, Pb) in Samoan lavas. *Earth and Planetary Science Letters*, 111(1), 183–199. [https://doi.org/10.1016/0012-821X\(92\)90178-X](https://doi.org/10.1016/0012-821X(92)90178-X)
- Fitton, J. G., Saunders, A. D., Kempton, P. D., & Hardarson, B. S. (2003). Does depleted mantle form an intrinsic part of the Iceland plume?: ICELAND PLUME. *Geochemistry, Geophysics, Geosystems*, 4(3), 1032. <https://doi.org/10.1029/2002GC000424>
- Francis, D. (1985). The Baffin Bay lavas and the value of picrites as analogues of primary magmas. *Contributions to Mineralogy and Petrology*, 89(2–3), 144–154. <https://doi.org/10.1007/BF00379449>
- Gale, A., Dalton, C. A., Langmuir, C. H., Su, Y., & Schilling, J.-G. (2013). The mean composition of ocean ridge basalts. *Geochemistry, Geophysics, Geosystems*, 14, 489–518. <https://doi.org/10.1029/2012GC004334>
- Garapić, G., Mallik, A., Dasgupta, R., & Jackson, M. G. (2015). Oceanic lavas sampling the high- $^3\text{He}/^4\text{He}$ mantle reservoir: Primitive, depleted, or re-enriched? *American Mineralogist*, 100(10), 2066–2081. <https://doi.org/10.2138/am-2015-5154>
- Garnero, E. J., & McNamara, A. K. (2008). Structure and dynamics of Earth's lower mantle. *Science*, 320(5876), 626–628. <https://doi.org/10.1126/science.1148028>
- Garnero, E. J., McNamara, A. K., & Shim, S.-H. (2016). Continent-sized anomalous zones with low seismic velocity at the base of Earth's mantle. *Nature Geoscience*, 9(7), 481–489. <https://doi.org/10.1038/ngeo2733>
- Graham, D. W., Christie, D. M., Harpp, K. S., & Lupton, J. E. (1993). Mantle plume helium in submarine basalts from the Galápagos Platform. *Science*, 262(5142), 2023–2026. <https://doi.org/10.1126/science.262.5142.2023>
- Graham, D. W. (2002). Noble gas isotope geochemistry of mid-ocean ridge and ocean island basalts: Characterization of mantle source reservoirs. *Reviews in Mineralogy and Geochemistry*, 47(1), 247–317. <https://doi.org/10.2138/rmg.2002.47.8>
- Graham, D. W., Larsen, L. M., Hanan, B. B., Storey, M., Pedersen, A. K., & Lupton, J. E. (1998). Helium isotope composition of the early Iceland mantle plume inferred from the Tertiary picrites of West Greenland. *Earth and Planetary Science Letters*, 160(3–4), 241–255. [https://doi.org/10.1016/s0012-821x\(98\)00083-1](https://doi.org/10.1016/s0012-821x(98)00083-1)
- Hanan, B. B., & Graham, D. W. (1996). Lead and helium isotope evidence from oceanic basalts for a common deep source of mantle plumes. *Science (New York, N.Y.)*, 272(5264), 991–995.
- Harðardóttir, S., Halldórsson, S. A., & Hilton, D. R. (2018). Spatial distribution of helium isotopes in Icelandic geothermal fluids and volcanic materials with implications for location, upwelling and evolution of the Icelandic mantle plume. *Chemical Geology*, 480, 12–27. <https://doi.org/10.1016/j.chemgeo.2017.05.012>
- Hardarson, B. S., Fitton, J. G., Ellam, R. M., & Pringle, M. S. (1997). Rift relocation—A geochemical and geochronological investigation of a palaeo-rift in northwest Iceland. *Earth and Planetary Science Letters*, 153(3), 181–196. [https://doi.org/10.1016/S0012-821X\(97\)00145-3](https://doi.org/10.1016/S0012-821X(97)00145-3)
- Hart, S. R., & Gaetani, G. A. (2006). Mantle Pb paradoxes: The sulfide solution. *Contributions to Mineralogy and Petrology*, 152(3), 295–308. <https://doi.org/10.1007/s00410-006-0108-1>
- Hart, S. R., Hauri, E. H., Oschmann, L. A., & Whitehead, J. A. (1992). Mantle plumes and entrainment: Isotopic evidence. *Science*, 256(5056), 517–520. <https://doi.org/10.1126/science.256.5056.517>
- Hays, M. R. (2004). Intra-transform volcanism along the Siqueiros fracture zone $8^\circ 20'–8^\circ 30'N$, East Pacific Rise, Master of Science Thesis, University of Florida.

- Heber, V. S., Brooker, R. A., Kelley, S. P., & Wood, B. J. (2007). Crystal–melt partitioning of noble gases (helium, neon, argon, krypton, and xenon) for olivine and clinopyroxene. *Geochimica et Cosmochimica Acta*, 71(4), 1041–1061. <https://doi.org/10.1016/j.gca.2006.11.010>
- Hervig, R. L., Smith, J. V., & Dawson, J. B. (1986). Lherzolite xenoliths in kimberlites and basalts: Petrogenetic and crystallochemical significance of some minor and trace elements in olivine, pyroxenes, garnet and spinel. *Earth and Environmental Science Transactions of the Royal Society of Edinburgh*, 77(3), 181–201. <https://doi.org/10.1017/S026359330001083X>
- Herzberg, C., & Asimow, P. D. (2015). PRIMELT3 MEGA.XLSM software for primary magma calculation: Peridotite primary magma MgO contents from the liquidus to the solidus. *Geochemistry, Geophysics, Geosystems*, 16, 563–578. <https://doi.org/10.1002/2014GC005631>
- Herzberg, C., Asimow, P. D., Ionov, D. A., Vidito, C., Jackson, M. G., & Geist, D. (2013). Nickel and helium evidence for melt above the core–mantle boundary. *Nature*, 493(7432), 393–397. <https://doi.org/10.1038/nature11771>
- Herzberg, C., & Gazel, E. (2009). Petrological evidence for secular cooling in mantle plumes. *Nature*, 458(7238), 619–622. <https://doi.org/10.1038/nature07857>
- Hilton, D. R., Barling, J., & Wheller, G. E. (1995). Effect of shallow-level contamination on the helium isotope systematics of ocean-island lavas. *Nature*, 373(6512), 330–333. <https://doi.org/10.1038/373330a0>
- Hilton, D. R., Grönvold, K., Macpherson, C. G., & Castillo, P. R. (1999). Extreme ${}^3\text{He}/{}^4\text{He}$ ratios in northwest Iceland: Constraining the common component in mantle plumes. *Earth and Planetary Science Letters*, 173(1–2), 53–60. [https://doi.org/10.1016/S0012-821X\(99\)00215-0](https://doi.org/10.1016/S0012-821X(99)00215-0)
- Hofmann, A. W. (1997). Mantle geochemistry: The message from oceanic volcanism. *Nature*, 385(6613), 219. <https://doi.org/10.1038/385219a0>
- Hofmann, A. W. (2003). Sampling mantle heterogeneity through oceanic basalts: Isotopes and trace elements. *Treatise on Geochemistry*, 2, 568. <https://doi.org/10.1016/B0-08-043751-6/02123-X>
- Hofmann, A. W., Jochum, K. P., Seufert, M., & White, W. M. (1986). Nb and Pb in oceanic basalts: New constraints on mantle evolution. *Earth and Planetary Science Letters*, 79(1–2), 33–45. [https://doi.org/10.1016/0012-821X\(86\)90038-5](https://doi.org/10.1016/0012-821X(86)90038-5)
- Hofmann, A. W., & White, W. M. (1983). Ba, Rb, and Cs in the Earth's mantle. *Zeitschrift Naturforschung Teil A*, 38, 256–266. <https://doi.org/10.1515/zna-1983-0225>
- Hole, M. J., & Millett, J. M. (2016). Controls of mantle potential temperature and lithospheric thickness on magmatism in the North Atlantic Igneous Province. *Journal of Petrology*, 57(2), 417–436. <https://doi.org/10.1093/petrology/egw014>
- Holm, P. M., Gill, R. C. O., Pedersen, A. K., Larsen, J. G., Hald, N., Nielsen, T. F. D., & Thirlwall, M. F. (1993). The Tertiary picrites of West Greenland: Contributions from 'Icelandic' and other sources. *Earth and Planetary Science Letters*, 115(1–4), 227–244. [https://doi.org/10.1016/0012-821X\(93\)90224-W](https://doi.org/10.1016/0012-821X(93)90224-W)
- Horan, M. F., Carlson, R. W., Walker, R. J., Jackson, M., Garçon, M., & Norman, M. (2018). Tracking Hadean processes in modern basalts with 142-Neodymium. *Earth and Planetary Science Letters*, 484, 184–191. <https://doi.org/10.1016/j.epsl.2017.12.017>
- Jackson, C. R. M., Parman, S. W., Kelley, S. P., & Cooper, R. F. (2013). Constraints on light noble gas partitioning at the conditions of spinel–peridotite melting. *Earth and Planetary Science Letters*, 384, 178–187. <https://doi.org/10.1016/j.epsl.2013.09.046>
- Jackson, M. G., Hart, S. R., Saal, A. E., Shimizu, N., Kurz, M. D., Blusztajn, J. S., & Skovgaard, A. C. (2008). Globally elevated titanium, tantalum, and niobium (TITAN) in ocean island basalts with high ${}^3\text{He}/{}^4\text{He}$. *Geochemistry, Geophysics, Geosystems*, 9, Q04027. <https://doi.org/10.1029/2007GC001876>
- Jackson, M. G., Konter, J. G., & Becker, T. W. (2017). Primordial helium entrained by the hottest mantle plumes. *Nature*, 542(7641), 340–343. <https://doi.org/10.1038/nature21023>
- Jackson, M. G., Kurz, M. D., Hart, S. R., & Workman, R. K. (2007). New Samoan lavas from Ofu Island reveal a hemispherically heterogeneous high ${}^3\text{He}/{}^4\text{He}$ mantle. *Earth and Planetary Science Letters*, 264(3–4), 360–374. <https://doi.org/10.1016/j.epsl.2007.09.023>
- Jackson, M. G., Carlson, R. W., Kurz, M. D., Kempton, P. D., Francis, D., & Blusztajn, J. (2010). Evidence for the survival of the oldest terrestrial mantle reservoir. *Nature*, 466(7308), 853–856. <https://doi.org/10.1038/nature09287>
- Jackson, M. G., Hart, S. R., Koppers, A. A. P., Staudigel, H., Konter, J., Blusztajn, J., et al. (2007). The return of subducted continental crust in Samoan lavas. *Nature*, 448(7154), 684–687. <https://doi.org/10.1038/nature06048>
- Jackson, M. G., & Shirey, S. B. (2011). Re–Os isotope systematics in Samoan shield lavas and the use of Os-isotopes in olivine phenocrysts to determine primary magmatic compositions. *Earth and Planetary Science Letters*, 312(1–2), 91–101. <https://doi.org/10.1016/j.epsl.2011.09.046>
- Jellinek, A. M., & Manga, M. (2004). Links between long-lived hot spots, mantle plumes, D'', and plate tectonics. *Reviews of Geophysics*, 42, RG3002. <https://doi.org/10.1029/2003RG000144>
- Jenner, F. E., & O'Neill, H. S. C. (2012). Analysis of 60 elements in 616 ocean floor basaltic glasses. *Geochemistry, Geophysics, Geosystems*, 13, Q02005. <https://doi.org/10.1029/2011GC004009>
- Jephcoat, A. P. (1998). Rare-gas solids in the Earth's deep interior. *Nature*, 393(6683), 355–358. <https://doi.org/10.1038/30712>
- Jochum, K. P., Weis, U., Schwager, B., Stoll, B., Wilson, S. A., Haug, G. H., et al. (2016). Reference values following ISO guidelines for frequently requested rock reference materials. *Geostandards and Geoanalytical Research*, 40(3), 333–350. <https://doi.org/10.1111/j.1751-908X.2015.00392.x>
- Keen, C. E., Dickie, K., & Dehler, S. A. (2012). The volcanic margins of the northern Labrador Sea: Insights to the rifting process: Volcanic margins, northern Labrador Sea. *Tectonics*, 31, L04301. <https://doi.org/10.1029/2011TC002985>
- Kent, A. J. R., Stolper, E. M., Francis, D., Woodhead, J., Frei, R., & Eiler, J. (2004). Mantle heterogeneity during the formation of the North Atlantic Igneous Province: Constraints from trace element and Sr-Nd-Os-O isotope systematics of Baffin Island picrites: NORTH ATLANTIC IGNEOUS PROVINCE. *Geochemistry, Geophysics, Geosystems*, 5, Q11004. <https://doi.org/10.1029/2004GC000743>
- King, S. D., & Adam, C. (2014). Hotspot swells revisited. *Physics of the Earth and Planetary Interiors*, 235, 66–83. <https://doi.org/10.1016/j.pepi.2014.07.006>
- Klein, E. M., & Langmuir, C. H. (1987). Global correlations of ocean ridge basalt chemistry with axial depth and crustal thickness. *Journal of Geophysical Research*, 92(B8), 8089. <https://doi.org/10.1029/JB092iB08p08089>
- Köhler, T. P., & Brey, G. P. (1990). Calcium exchange between olivine and clinopyroxene calibrated as a geothermobarometer for natural peridotites from 2 to 60 kb with applications. *Geochimica et Cosmochimica Acta*, 54(9), 2375–2388. [https://doi.org/10.1016/0016-7037\(90\)90226-B](https://doi.org/10.1016/0016-7037(90)90226-B)
- Konter, J. G., & Becker, T. W. (2012). Shallow lithospheric contribution to mantle plumes revealed by integrating seismic and geochemical data: Seismic and geochemical correlations. *Geochemistry, Geophysics, Geosystems*, 13, Q02004. <https://doi.org/10.1029/2011GC003923>

- Kruijer, T. S., & Kleine, T. (2018). No ^{182}W excess in the Ontong Java Plateau source. *Chemical Geology*, 485, 24–31. <https://doi.org/10.1016/j.chemgeo.2018.03.024>
- Kurz, M. D., Jenkins, W. J., & Hart, S. R. (1982). Helium isotopic systematics of oceanic islands and mantle heterogeneity. *Nature*, 297(5861), 43–47. <https://doi.org/10.1038/297043a0>
- Kurz, M. D. (1986). Cosmogenic helium in a terrestrial igneous rock. *Nature*, 320(6061), 435. <https://doi.org/10.1038/320435a0>
- Kurz, M. D., & Geist, D. (1999). Dynamics of the Galapagos hotspot from helium isotope geochemistry. *Geochimica et Cosmochimica Acta*, 63(23), 4139–4156. [https://doi.org/10.1016/S0016-7037\(99\)00314-2](https://doi.org/10.1016/S0016-7037(99)00314-2)
- Kurz, M. D., Jenkins, W. J., Hart, S. R., & Clague, D. (1983). Helium isotopic variations in volcanic rocks from Loihi Seamount and the Island of Hawaii. *Earth and Planetary Science Letters*, 66, 388–406. [https://doi.org/10.1016/0012-821X\(83\)90154-1](https://doi.org/10.1016/0012-821X(83)90154-1)
- Kurz, M. D., Rowland, S. K., Curtice, J., Saal, A. E., & Naumann, T. (2014). Eruption rates for Fernandina Volcano. In *The Galápagos: A Natural Laboratory for the Earth Sciences* (pp. 41–54). Washington, DC: American Geophysical Union. <https://doi.org/10.1002/9781118852538.ch4>
- Larsen, L. M., & Pedersen, A. K. (2009). Petrology of the Paleocene picrites and flood basalts on Disko and Nuussuaq, West Greenland. *Journal of Petrology*, 50(9), 1667–1711. <https://doi.org/10.1093/petrology/egp048>
- Larsen, L. M., & Pedersen, A. K. (2000). Processes in high-Mg, high-T magmas: Evidence from olivine, chromite and glass in Palaeogene picrites from West Greenland. *Journal of Petrology*, 41(7), 1071–1098. <https://doi.org/10.1093/petrology/41.7.1071>
- Lawver, L. A., & Müller, R. D. (1994). Iceland hotspot track. *Geology*, 22(4), 311–314. [https://doi.org/10.1130/0091-7613\(1994\)022<0311:IHT>2.3.CO;2](https://doi.org/10.1130/0091-7613(1994)022<0311:IHT>2.3.CO;2)
- Lekic, V., Cottaar, S., Dziewonski, A., & Romanowicz, B. (2012). Cluster analysis of global lower mantle tomography: A new class of structure and implications for chemical heterogeneity. *Earth and Planetary Science Letters*, 357–358, 68–77. <https://doi.org/10.1016/j.epsl.2012.09.014>
- Li, M., McNamara, A. K., & Garnero, E. J. (2014). Chemical complexity of hotspots caused by cycling oceanic crust through mantle reservoirs. *Nature Geoscience*, 7(5), 366–370. <https://doi.org/10.1038/ngeo2120>
- Lightfoot, P. C., Hawkesworth, C. J., Olshesky, K., Green, T., Doherty, W., & Keays, R. R. (1997). Geochemistry of Tertiary tholeiites and picrites from Qeqertarsuuaq (Disko Island) and Nuussuaq, West Greenland with implications for the mineral potential of comagmatic intrusions. *Contributions to Mineralogy and Petrology*, 128(2–3), 139–163. <https://doi.org/10.1007/s004100050300>
- Loewen, M. W., Graham, D. W., Bindeman, I. N., Lupton, J. E., & Garcia, M. O. (2019). Hydrogen isotopes in high $^3\text{He}/^4\text{He}$ submarine basalts: Primordial vs. recycled water and the veil of mantle enrichment. *Earth and Planetary Science Letters*, 508, 62–73. <https://doi.org/10.1016/j.epsl.2018.12.012>
- Macpherson, C., Hilton, D., Day, J., Lowry, D., & Gronvold, K. (2005). High- $^3\text{He}/^4\text{He}$, depleted mantle and low- $\delta^{18}\text{O}$, recycled oceanic lithosphere in the source of central Iceland magmatism. *Earth and Planetary Science Letters*, 233(3–4), 411–427. <https://doi.org/10.1016/j.epsl.2005.02.037>
- Madrigal, P., Gazel, E., Flores, K. E., Bizimis, M., & Jicha, B. (2016). Record of massive upwellings from the Pacific large low shear velocity province. *Nature Communications*, 7(1), 13,309. <https://doi.org/10.1038/ncomms13309>
- Marty, B., Upton, B. G. J., & Ellam, R. M. (1998). Helium isotopes in early Tertiary basalts, northeast Greenland: Evidence for 58 Ma plume activity in the North Atlantic–Iceland volcanic province. *Geology*, 26(5), 407–410. [https://doi.org/10.1130/0091-7613\(1998\)026<0407:HIETB>2.3.CO;2](https://doi.org/10.1130/0091-7613(1998)026<0407:HIETB>2.3.CO;2)
- Matthey, D., Lowry, D., & Macpherson, C. (1994). Oxygen isotope composition of mantle peridotite. *Earth and Planetary Science Letters*, 128(3–4), 231–241. [https://doi.org/10.1016/0012-821X\(94\)90147-3](https://doi.org/10.1016/0012-821X(94)90147-3)
- McCoy-West, A. J., Fitton, J. G., Pons, M.-L., Inglis, E. C., & Williams, H. M. (2018). The Fe and Zn isotope composition of deep mantle source regions: Insights from Baffin Island picrites. *Geochimica et Cosmochimica Acta*, 238, 542–562. <https://doi.org/10.1016/j.gca.2018.07.021>
- McDonough, W. F., & Sun, S. (1995). The composition of the Earth. *Chemical Geology*, 120(3), 223–253. [https://doi.org/10.1016/0009-2541\(94\)00140-4](https://doi.org/10.1016/0009-2541(94)00140-4)
- McDougall, I., Kristjansson, L., & Saemundsson, K. (1984). Magnetostratigraphy and geochronology of northwest Iceland. *Journal of Geophysical Research*, 89(B8), 7029–7060. <https://doi.org/10.1029/JB089iB08p07029>
- McNamara, A. K. (2019). A review of large low shear velocity provinces and ultra low velocity zones. *Tectonophysics*, 760, 199–220. <https://doi.org/10.1016/j.tecto.2018.04.015>
- McNamara, A. K., Garnero, E. J., & Rost, S. (2010). Tracking deep mantle reservoirs with ultra-low velocity zones. *Earth and Planetary Science Letters*, 299(1–2), 1–9. <https://doi.org/10.1016/j.epsl.2010.07.042>
- Moreira, M., Kanzari, A., & Madureira, P. (2012). Helium and neon isotopes in São Miguel island basalts, Azores Archipelago: New constraints on the “low ^3He ” hotspot origin. *Chemical Geology*, 322–323, 91–98. <https://doi.org/10.1016/j.chemgeo.2012.06.014>
- Mukhopadhyay, S. (2012). Early differentiation and volatile accretion recorded in deep-mantle neon and xenon. *Nature*, 486(7401), 101–104. <https://doi.org/10.1038/nature11141>
- Mukhopadhyay, S., & Parai, R. (2019). Noble gases: A record of Earth’s evolution and mantle dynamics. *Annual Review of Earth and Planetary Sciences*, 47(1), 389–419. <https://doi.org/10.1146/annurev-earth-053018-060238>
- Mundl, A., Touboul, M., Jackson, M. G., Day, J. M. D., Kurz, M. D., Lekic, V., & Walker, R. J. (2017). Tungsten-182 heterogeneity in modern ocean island basalts. *Science*, 356(6333), 66–69. <https://doi.org/10.1126/science.aaal4179>
- Mundl-Petermeier, A., Walker, R. J., Jackson, M. G., Blachert-Toft, J., Kurz, M. D., & Halldórrsson, S. A. (2019). Temporal evolution of primordial tungsten-182 and $^3\text{He}/^4\text{He}$ signatures in the Iceland mantle plume. *Chemical Geology*, 525, 245–259. <https://doi.org/10.1016/j.chemgeo.2019.07.026>
- Parman, S. W., Kurz, M. D., Hart, S. R., & Grove, T. L. (2005). Helium solubility in olivine and implications for high $^3\text{He}/^4\text{He}$ in ocean island basalts. *Nature*, 437(7062), 1140–1143. <https://doi.org/10.1038/nature04215>
- Peate, D. W. (2003). The Prinsen af Wales Bjerge formation lavas, East Greenland: The transition from tholeiitic to alkalic magmatism during Palaeogene continental break-up. *Journal of Petrology*, 44(2), 279–304. <https://doi.org/10.1093/petrology/44.2.279>
- Perfit, M. R., Fornari, D. J., Ridley, W. I., Kirk, P. D., Casey, J., Kastens, K. A., et al. (1996). Recent volcanism in the Siqueiros transform fault: Picritic basalts and implications for MORB magma genesis. *Earth and Planetary Science Letters*, 141(1–4), 91–108. [https://doi.org/10.1016/0012-821X\(96\)00052-0](https://doi.org/10.1016/0012-821X(96)00052-0)
- Peters, B. J., Carlson, R. W., Day, J. M. D., & Horan, M. F. (2018). Hadean silicate differentiation preserved by anomalous $^{142}\text{Nd}/^{144}\text{Nd}$ ratios in the Réunion hotspot source. *Nature*, 555(7694), 89–93. <https://doi.org/10.1038/nature25754>
- Pető, M. K., Mukhopadhyay, S., & Kelley, K. A. (2013). Heterogeneities from the first 100 million years recorded in deep mantle noble gases from the Northern Lau Back-arc Basin. *Earth and Planetary Science Letters*, 369–370, 13–23. <https://doi.org/10.1016/j.epsl.2013.02.012>

- Porcelli, D., & Halliday, A. N. (2001). The core as a possible source of mantle helium. *Earth and Planetary Science Letters*, 192(1), 45–56. [https://doi.org/10.1016/S0012-821X\(01\)00418-6](https://doi.org/10.1016/S0012-821X(01)00418-6)
- Price, A. A., Jackson, M. G., Blöcher-Toft, J., Blusztajn, J., Conatser, C. S., Konter, J. G., et al. (2016). Geochemical evidence in the northeast Lau Basin for subduction of the Cook-Austral volcanic chain in the Tonga Trench. *Geochemistry, Geophysics, Geosystems*, 17, 1694–1724. <https://doi.org/10.1002/2015GC006237>
- Putirka, K. (2008). Excess temperatures at ocean islands: Implications for mantle layering and convection. *Geology*, 36(4), 283–286. <https://doi.org/10.1130/G24615A.1>
- Putirka, K., Tao, Y., Hari, K. R., Perfit, M. R., Jackson, M. G., & Arevalo, R. (2018). The mantle source of thermal plumes: Trace and minor elements in olivine and major oxides of primitive liquids (and why the olivine compositions don't matter). *American Mineralogist*, 103(8), 1253–1270. <https://doi.org/10.2138/am-2018-6192>
- Putirka, K. D., Perfit, M., Ryerson, F. J., & Jackson, M. G. (2007). Ambient and excess mantle temperatures, olivine thermometry, and active vs. Passive upwelling. *Chemical Geology*, 241(3–4), 177–206. <https://doi.org/10.1016/j.chemgeo.2007.01.014>
- Rizo, H., Andrault, D., Bennett, N. R., Humayun, M., Brandon, A., Vlastelic, I., & Murphy, D. T. (2019). 182 W evidence for core-mantle interaction in the source of mantle plumes. *Geochemical Perspectives Letters*, 11, 6–11. <https://doi.org/10.7185/geochemlet.1917>
- Rizo, H., Walker, R. J., Carlson, R. W., Horan, M. F., Mukhopadhyay, S., Manthos, V., & Jackson, M. G. (2016). Preservation of Earth-forming events in the tungsten isotopic composition of modern flood basalts. *Science*, 352(6287), 809–812. <https://doi.org/10.1126/science.aad8563>
- Robillard, I., Francis, D., & Ludden, J. N. (1992). The relationship between E- and N-type magmas in the Baffin Bay Lavas. *Contributions to Mineralogy and Petrology*, 112(2–3), 230–241. <https://doi.org/10.1007/BF00310457>
- Rost, S., Garnero, E. J., Williams, Q., & Manga, M. (2005). Seismological constraints on a possible plume root at the core–mantle boundary. *Nature*, 435(7042), 666–669. <https://doi.org/10.1038/nature03620>
- Roth, A. S. G., Liebske, C., Maden, C., Burton, K. W., Schönbächler, M., & Busemann, H. (2019). The primordial He budget of the Earth set by percolative core formation in planetesimals. *Geochemical Perspectives Letters*, 26–31. <https://doi.org/10.7185/geochemlet.1901>
- Rudnick, R. L., & Gao, S. (2003). Composition of the continental crust. In R. L. Rudnick (Ed.), *Treatise on Geochemistry, The Crust* (Vol. 3, pp. 1–64). Elsevier. <https://doi.org/10.1016/B0-08-043751-6/03016-4>
- Saal, A., Kurz, M., Hart, S., Blusztajn, J., Blöcher-Toft, J., Liang, Y., & Geist, D. (2007). The role of lithospheric gabbros on the composition of Galapagos lavas. *Earth and Planetary Science Letters*, 257(3–4), 391–406. <https://doi.org/10.1016/j.epsl.2007.02.040>
- Samuel, H., & Farnetani, C. G. (2003). Thermochemical convection and helium concentrations in mantle plumes. *Earth and Planetary Science Letters*, 207(1–4), 39–56. [https://doi.org/10.1016/S0012-821X\(02\)01125-1](https://doi.org/10.1016/S0012-821X(02)01125-1)
- Saunders, A. D., Kerr, A. C., Norry, M. J., & Kent, R. W. (1997). The North Atlantic igneous province. 100, 45–93.
- Shorttle, O., MacLennan, J., & Lambart, S. (2014). Quantifying lithological variability in the mantle. *Earth and Planetary Science Letters*, 395, 24–40. <https://doi.org/10.1016/j.epsl.2014.03.040>
- Starkey, N. A., Fitton, J. G., Stuart, F. M., & Larsen, L. M. (2012). Melt inclusions in olivines from early Iceland plume picrites support high $^3\text{He}/^4\text{He}$ in both enriched and depleted mantle. *Chemical Geology*, 306–307, 54–62. <https://doi.org/10.1016/j.chemgeo.2012.02.022>
- Starkey, N. A., Stuart, F. M., Ellam, R. M., Fitton, J. G., Basu, S., & Larsen, L. M. (2009). Helium isotopes in early Iceland plume picrites: Constraints on the composition of high $^3\text{He}/^4\text{He}$ mantle. *Earth and Planetary Science Letters*, 277(1–2), 91–100. <https://doi.org/10.1016/j.epsl.2008.10.007>
- St-Onge, M. R., Van Gool, J. A. M., Garde, A. A., & Scott, D. J. (2009). Correlation of Archaean and Palaeoproterozoic units between northeastern Canada and western Greenland: Constraining the pre-collisional upper plate accretionary history of the Trans-Hudson orogen. *Geological Society, London, Special Publications*, 318(1), 193–235. <https://doi.org/10.1144/SP318.7>
- Storey, M., Duncan, R. A., Pedersen, A. K., Larsen, L. M., & Larsen, H. C. (1998). $^{40}\text{Ar}/^{39}\text{Ar}$ geochronology of the West Greenland Tertiary volcanic province. *Earth and Planetary Science Letters*, 160(3–4), 569–586. [https://doi.org/10.1016/S0012-821X\(98\)00112-5](https://doi.org/10.1016/S0012-821X(98)00112-5)
- Stuart, F. M., Ellam, R. M., Harrop, P. J., Fitton, J. G., & Bell, B. R. (2000). Constraints on mantle plumes from the helium isotopic composition of basalts from the British Tertiary igneous province. *Earth and Planetary Science Letters*, 177(3), 273–285. [https://doi.org/10.1016/S0012-821X\(00\)00050-9](https://doi.org/10.1016/S0012-821X(00)00050-9)
- Stuart, F. M., Lass-Evans, S., Godfrey Fitton, J., & Ellam, R. M. (2003). High $^3\text{He}/^4\text{He}$ ratios in picritic basalts from Baffin Island and the role of a mixed reservoir in mantle plumes. *Nature*, 424(6944), 57–59. <https://doi.org/10.1038/nature01711>
- Tackley, P. J. (2000). Mantle convection and plate tectonics: Toward an integrated physical and chemical theory. *Science*, 288(5473), 2002–2007. <https://doi.org/10.1126/science.288.5473.2002>
- Treila, J., Gazel, E., Sobolev, A. V., Moore, L., Bizimis, M., Jicha, B., & Batanova, V. G. (2017). The hottest lavas of the Phanerozoic and the survival of deep Archaean reservoirs. *Nature Geoscience*, 10(6), 451–456. <https://doi.org/10.1038/NGEO2954>
- Treila, J., Vidito, C., Gazel, E., Herzberg, C., Class, C., Whalen, W., et al. (2015). Recycled crust in the Galápagos Plume source at 70 Ma: Implications for plume evolution. *Earth and Planetary Science Letters*, 425, 268–277. <https://doi.org/10.1016/j.epsl.2015.05.036>
- Valbracht, P. J., Staudacher, T., Malahoff, A., & Allègre, C. J. (1997). Noble gas systematics of deep rift zone glasses from Loihi Seamount, Hawaii. *Earth and Planetary Science Letters*, 150(3), 399–411. [https://doi.org/10.1016/S0012-821X\(97\)00094-0](https://doi.org/10.1016/S0012-821X(97)00094-0)
- Walter, M. J. (1998). Melting of garnet peridotite and the origin of komatiite and depleted lithosphere. *Journal of Petrology*, 39(1), 29–60. <https://doi.org/10.1093/petroj/39.1.29>
- Wheeler, J. O., Hoffman, P. F., Card, K. D., Davidson, A., Sandford, B. V., Okulitch, A. V., & Roest, W. R. (1996). Geologic map of Canada, scale 1:5 000 000. Geological Survey of Canada Map, 1860A.
- White, W. M. (2015). Isotopes, DUPAL, LLSVPs, and Anekantavada. *Chemical Geology*, 419, 10–28. <https://doi.org/10.1016/j.chemgeo.2015.09.026>
- Williams, C. D., Mukhopadhyay, S., Rudolph, M. L., & Romanowicz, B. (2019). Primitive helium is sourced from seismically slow regions in the lowermost mantle. *Geochemistry, Geophysics, Geosystems*, 20, 4130–4145. <https://doi.org/10.1029/2019GC008437>
- Workman, R. K., Hart, S. R., Jackson, M., Regelous, M., Farley, K. A., Blusztajn, J., & Staudigel, H. (2004). Recycled metasomatized lithosphere as the origin of the enriched mantle II (EM2) end-member: Evidence from the Samoan volcanic chain. *Geochemistry, Geophysics, Geosystems*, 5, Q04008. <https://doi.org/10.1029/2003GC000623>
- Yaxley, G. M., Kamenetsky, V. S., Kamenetsky, M., Norman, M. D., & Francis, D. (2004). Origins of compositional heterogeneity in olivine-hosted melt inclusions from the Baffin Island picrites. *Contributions to Mineralogy and Petrology*, 148(4), 426–442. <https://doi.org/10.1007/s00410-004-0613-z>
- Zindler, A., & Hart, S. (1986). Chemical geodynamics. *Annual Review of Earth and Planetary Sciences*, 14(1), 493–571. <https://doi.org/10.1146/annurev.ea.14.050186.002425>

References From the Supporting Information

- Bindeman, I., Gurenko, A., Sigmarsdóttir, O., & Chaussidon, M. (2008). Oxygen isotope heterogeneity and disequilibria of olivine crystals in large volume Holocene basalts from Iceland: Evidence for magmatic digestion and erosion of Pleistocene hyaloclastites. *Geochimica et Cosmochimica Acta*, 72(17), 4397–4420. <https://doi.org/10.1016/j.gca.2008.06.010>
- Blichert-Toft, J., Chauvel, C., & Albarède, F. (1997). Separation of Hf and Lu for high-precision isotope analysis of rock samples by magnetic sector-multiple collector ICP-MS. *Contributions to Mineralogy and Petrology*, 127(3), 248–260. <https://doi.org/10.1007/s004100050278>
- Blichert-Toft, J., & Albarède, F. (2009). Mixing of isotopic heterogeneities in the Mauna Kea plume conduit. *Earth and Planetary Science Letters*, 282(1), 190–200. <https://doi.org/10.1016/j.epsl.2009.03.015>
- Bouvier, A., & Boyet, M. (2016). Primitive solar system materials and Earth share a common initial ^{142}Nd abundance. *Nature*, 537(7620), 399–402. <https://doi.org/10.1038/nature19351>
- Burkhardt, C., Borg, L. E., Brennecke, G. A., Shollenberger, Q. R., Dauphas, N., & Kleine, T. (2016). A nucleosynthetic origin for the Earth's anomalous ^{142}Nd composition. *Nature*, 537(7620), 394–398. <https://doi.org/10.1038/nature18956>
- Carlson, R. W. (2019). Analysis of lunar samples: Implications for planet formation and evolution. *Science*, 365(6450), 240–243. <https://doi.org/10.1126/science.aaw7580>
- Eisele, J., Abouchami, W., Galer, S. J. G., & Hofmann, A. W. (2003). The 320 kyr Pb isotope evolution of Mauna Kea lavas recorded in the HSDP-2 drill core. *Geochemistry, Geophysics, Geosystems*, 4(2), 8710. <https://doi.org/10.1029/2002GC000339>
- Gannoun, A., Boyet, M., Rizo, H., & Goresky, A. E. (2011). ^{146}Sm – ^{142}Nd systematics measured in enstatite chondrites reveals a heterogeneous distribution of ^{142}Nd in the solar nebula. *Proceedings of the National Academy of Sciences*, 108(19), 7693–7697. <https://doi.org/10.1073/pnas.1017332108>
- Garçon, M., Boyet, M., Carlson, R. W., Horan, M. F., Auclair, D., & Mock, T. D. (2018). Factors influencing the precision and accuracy of Nd isotope measurements by thermal ionization mass spectrometry. *Chemical Geology*, 476, 493–514. <https://doi.org/10.1016/j.chemgeo.2017.12.003>
- Hoernle, K., Rohde, J., Hauff, F., Garbe-Schönberg, D., Homrighausen, S., Werner, R., & Morgan, J. P. (2015). How and when plume zonation appeared during the 132 Myr evolution of the Tristan Hotspot. *Nature Communications*, 6(1), 7799. <https://doi.org/10.1038/ncomms8799>
- Jackson, M. G., & Carlson, R. W. (2011). An ancient recipe for flood-basalt genesis. *Nature*, 476(7360), 316–319. <https://doi.org/10.1038/nature10326>
- Johnson, D. M., Hooper, P. R., & Conrey, R. M. (1999). XRF Analysis of rocks and minerals for major and trace elements on a single low dilution Li-tetraborate fused bead. *Advances in X-Ray Analysis*, 41, 843–867.
- Kiseeva, E. S., & Wood, B. J. (2015). The effects of composition and temperature on chalcophile and lithophile element partitioning into magmatic sulphides. *Earth and Planetary Science Letters*, 424, 280–294. <https://doi.org/10.1016/j.epsl.2015.05.012>
- Knaack, C., Cornelius, S. B., & Hooper, P. R. (1994). Trace element analyses of rocks and minerals by ICP-MS, Open File Rep. Retrieved from <http://www.sees.wsu.edu/Geolab/note/icpms.html>
- Kurz, M. D., Curtice, J., Lott, D. E., & Solow, A. (2004). Rapid helium isotopic variability in Mauna Kea shield lavas from the Hawaiian Scientific Drilling Project. *Geochemistry, Geophysics, Geosystems*, 5, Q04G14. <https://doi.org/10.1029/2002GC000439>
- Kurz, M. D., Curtice, J., Fornari, D., Geist, D., & Moreira, M. (2009). Primitive neon from the center of the Galápagos hotspot. *Earth and Planetary Science Letters*, 286(1), 23–34. <https://doi.org/10.1016/j.epsl.2009.06.008>
- Larsen, L. M., Pedersen, A. K., Sundvold, B., & Frei, R. (2003). Alkali picrites formed by melting of old metasomatized lithospheric mantle: Man'itlat member, vaigat formation. *Palaeocene of West Greenland*, 44(1), 36.
- Price, A. A., Jackson, M. G., Blichert-Toft, J., Hall, P. S., Sinton, J. M., Kurz, M. D., & Blusztajn, J. (2014). Evidence for a broadly distributed Samoan-plume signature in the northern Lau and North Fiji Basins. *Geochemistry, Geophysics, Geosystems*, 15, 986–1008. <https://doi.org/10.1002/2013GC005061>
- Price, A. A., Jackson, M. G., Blichert-Toft, J., Kurz, M. D., Gill, J., Blusztajn, J., et al. (2017). Geodynamic implications for zonal and meridional isotopic patterns across the northern Lau and North Fiji Basins. *Geochemistry, Geophysics, Geosystems*, 18, 1013–1042. <https://doi.org/10.1002/2016GC006651>
- Takamasa, A., & Nakai, S. (2009). Contamination introduced during rock sample powdering: Effects from different mill materials on trace element contamination. *Geochemical Journal*, 43, 389–394. <https://doi.org/10.2343/geochemj.1.0032>
- Tanaka, T., Togashi, S., Kamioka, H., Amakawa, H., Kagami, H., Hamamoto, T., et al. (2000). JNdI-1: A neodymium isotopic reference in consistency with LaJolla neodymium. *Chemical Geology*, 168(3–4), 279–281. [https://doi.org/10.1016/S0009-2541\(00\)00198-4](https://doi.org/10.1016/S0009-2541(00)00198-4)
- Valley, J. W., Kitchen, N., Kohn, M. J., Niendorf, C. R., & Spicuzza, M. J. (1995). UWG-2, a garnet standard for oxygen isotope ratios: Strategies for high precision and accuracy with laser heating. *Geochimica et Cosmochimica Acta*, 59(24), 5223–5231. [https://doi.org/10.1016/0016-7037\(95\)00386-X](https://doi.org/10.1016/0016-7037(95)00386-X)
- Weis, D., Kieffer, B., Maerschalk, C., Barling, J., de Jong, J., Williams, G. A., et al. (2006). High-precision isotopic characterization of USGS reference materials by TIMS and MC-ICP-MS: Isotopic study of USGS reference materials. *Geochemistry, Geophysics, Geosystems*, 7, Q07005. <https://doi.org/10.1029/2006GC001283>
- Workman, R. K., & Hart, S. R. (2005). Major and trace element composition of the depleted MORB mantle (DMM). *Earth and Planetary Science Letters*, 231(1–2), 53–72. <https://doi.org/10.1016/j.epsl.2004.12.005>